

# Discovery of 9-Cyclopropylethynyl-2-((S)-1-[1,4]dioxan-2-ylmethoxy)-6,7-dihydropyrimido[6,1-a]isoquinolin-4-one (GLPG1205), a Unique GPR84 Negative Allosteric Modulator Undergoing Evaluation in a Phase II Clinical Trial

Frédéric Labéguère, Sonia Dupont, Luke Alvey, Florilène Soulas, Gregory Newsome, Amynata Tirera, Vanessa Quenehen, Thi Thu Trang Mai, Pierre Deprez, Roland Blanqué, Line Oste, Sandrine Le Tallec, Steve De Vos, Annick Hagers, Ann Vandeveld, Luc Nelles, Nele Vandervoort, Katja Conrath, Thierry Christophe, Ellen van der Aar, Emanuelle Wakselman, Didier Merciris, Céline Cottreaux, Cécile da Costa, Laurent Saniere, Philippe Clement-Lacroix, Laura Jenkins, Graeme Milligan, Stephen Fletcher, Reginald Brys, and Romain Gosmini\*



Cite This: *J. Med. Chem.* 2020, 63, 13526–13545



Read Online

ACCESS |



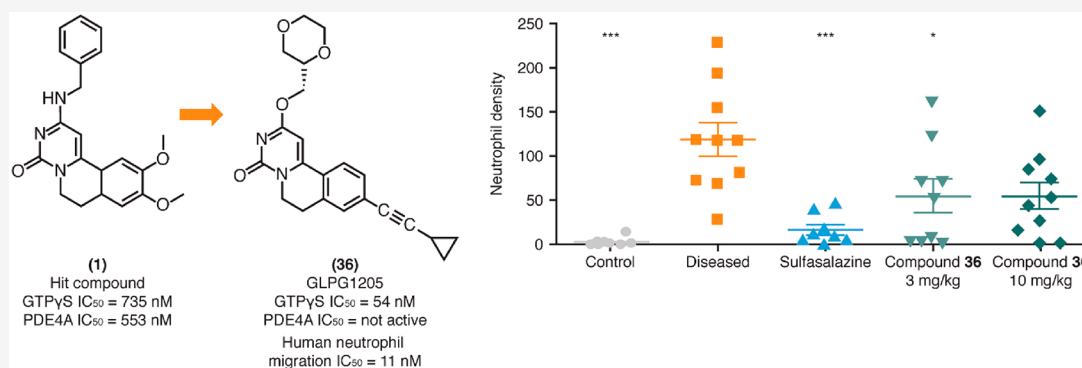
Metrics & More



Article Recommendations



Supporting Information



**ABSTRACT:** GPR84 is a medium chain free fatty acid-binding G-protein-coupled receptor associated with inflammatory and fibrotic diseases. As the only reported antagonist of GPR84 (PBI-4050) that displays relatively low potency and selectivity, a clear need exists for an improved modulator. Structural optimization of GPR84 antagonist hit 1, identified through high-throughput screening, led to the identification of potent and selective GPR84 inhibitor GLPG1205 (36). Compared with the initial hit, 36 showed improved potency in a guanosine 5'-O-[ $\gamma$ -thio]triphosphate assay, exhibited metabolic stability, and lacked activity against phosphodiesterase-4. This novel pharmacological tool allowed investigation of the therapeutic potential of GPR84 inhibition. At once-daily doses of 3 and 10 mg/kg, GLPG1205 reduced disease activity index score and neutrophil infiltration in a mouse dextran sodium sulfate-induced chronic inflammatory bowel disease model, with efficacy similar to positive-control compound sulfasalazine. The drug discovery steps leading to GLPG1205 identification, currently under phase II clinical investigation, are described herein.

## INTRODUCTION

GPR84 is a G-protein-coupled receptor (GPCR) that couples almost exclusively to pertussis-toxin sensitive G<sub>i/o</sub> pathways.<sup>1</sup> Whereas GPR84 has no unanimously accepted cognate ligand, medium-chain free fatty acids (MCFAs, carbon chain lengths of 9–14) have been known as agonists for over a decade<sup>1,2</sup> with decanoic acid (C10), undecanoic acid (C11), and lauric acid (C12) being the most effective.<sup>3</sup> An increasing range of synthetic GPR84 agonist ligands have been described, including embelin, 3,3'-diindolylmethane (DIM), 6-*n*-octylaminouracil (6-OAU),<sup>3</sup> and 2-(hexylthiol)pyrimidine-4,6 diol (2-HTP)<sup>4,5</sup> (Figure 1). These synthetic GPR84 ligands are

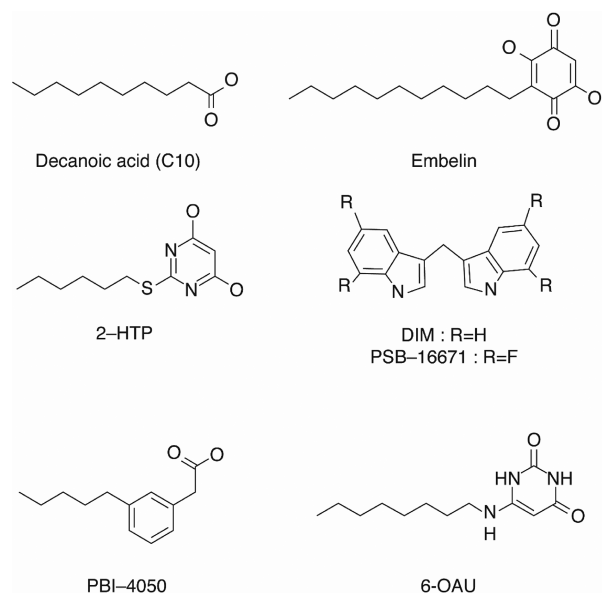
more potent than the MCFAs, with particular derivatives and structural relatives of 6-OAU being the most potent agonists of GPR84 to date.<sup>4–6</sup>

GPR84 is primarily expressed in innate immune cells (neutrophils,<sup>1,7</sup> monocytes,<sup>1</sup> macrophages,<sup>1,8</sup> dendritic cells,<sup>9</sup>

Received: February 14, 2020

Published: September 9, 2020





**Figure 1.** Chemical structures of known GPR84 agonists MCFA C10, embelin, 2-HTP, and DIM derivatives and the GPR84 antagonists PBI-4050 and 6-OAU. Abbreviations: 2-HTP, 2-(hexylthio)pyrimidine-4,6 diol; 6-OAU, 6-*n*-octylaminouracil; DIM, 3,3'-diindolylmethane; MCFA, medium-chain free fatty acids.

and microglia<sup>8,10</sup>) and splenic T and B cells.<sup>11</sup> Expression of GPR84 is highly upregulated by inflammatory stimuli in these innate immune cells and adipocytes,<sup>12</sup> suggesting an immunoregulatory role for the receptor.<sup>1,7,10–13</sup> In polymorphonuclear leukocytes and macrophages, activation of GPR84 results in chemotactic responses and enhances the release of cytokines (interleukin [IL]-8, IL-12, and tumor necrosis factor  $\alpha$  [TNF- $\alpha$ ]).<sup>1,3</sup> In addition, activation of this receptor in neutrophils and macrophages triggers the release of reactive oxygen species.<sup>14</sup>

GPR84 is suspected to be involved in inflammatory bowel disease (IBD), as increased levels of GPR84 messenger RNA (mRNA) have been observed in intestinal mucosal biopsies of patients with IBD (either ulcerative colitis or Crohn's disease).<sup>15</sup> Additionally, GPR84 may be involved in fibrotic processes, as one recent study observed that GPR84 knock-out mice display significantly reduced kidney fibrosis when compared with wild-type mice in an adenine-induced chronic kidney disease model.<sup>16</sup> Moreover, in a mouse bleomycin-induced pulmonary fibrosis model, treatment with the nonspecific GPR84 antagonist PBI-4050 reduced histological lesions in the lung by 47% compared with vehicle.<sup>16</sup> Other animal disease models have indicated a role for GPR84 in chronic pain,<sup>3</sup> reflux esophagitis,<sup>17</sup> acute myeloid leukemia,<sup>18</sup> obesity,<sup>19</sup> and Alzheimer's disease.<sup>9</sup> As such, GPR84 has emerged as a potential drug target, particularly for inflammatory and fibrotic diseases.

To date, only one low potency, nonspecific antagonist of GPR84 has been reported (PBI-4050), which inhibits GPR84  $G_{\alpha/i}$  activation initiated by either sodium decanoate or embelin.<sup>16</sup> In this article, we describe the discovery of GLPG1205 (36), a potent and selective GPR84 modulator, which demonstrates efficacy in *in vivo* IBD models and has been progressed in phase IIa clinical trials for the treatment of ulcerative colitis.

## RESULTS AND DISCUSSION

During the course of our investigations, there was limited structural information available to provide support with molecular modeling tools for identifying GPR84 antagonists. The closest homologs of GPR84 with resolved structures had sequence identities below 30%, thereby preventing homology models being developed with sufficient accuracy to enable structure-based design. Furthermore, ligand-based approaches were limited due to the absence of reference antagonists. These issues led us to rely on a high-throughput screen (HTS) approach to identify GPR84 antagonists.

A functional assay based on measurement of cyclic adenosine 3',5'-monophosphate (cAMP) was selected to detect antagonists from a collection of approximately 200 000 diverse compounds. The comparison of assay robustness between the cAMP assay and the orthogonal assay (<sup>35</sup>S]guanosine 5'-O-[ $\gamma$ -thio]triphosphate (GTP $\gamma$ S) binding) led us to use the GTP $\gamma$ S for hit confirmation and concentration–response determination. The GTP $\gamma$ S assay measures the level of G protein activation following agonist occupancy of a GPCR by determining the binding of the nonhydrolyzable analogue [<sup>35</sup>S]GTP $\gamma$ S to  $G_{\alpha}$  subunits using membranes derived from a HEK293 cell line stably over-expressing human GPR84.

Through HTS, the commercially available compound 2-(benzylamino)-9,10-dimethoxy-6,7-dihydro-4H-pyrimido[6,1-*a*]isoquinolin-4-one (**1**) (Table 1) was identified as an appropriate starting point with submicromolar potency ( $IC_{50}$  = 735 nM) combined with favorable druglikeness properties,<sup>20</sup> such as moderate lipophilicity (XlogP3 = 2.4), polar surface area (PSA = 63.2), and molecular weight (MW = 363.4).

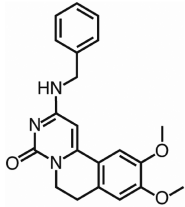
Compound **1** showed moderate *in vitro* metabolic clearance in both mouse and human microsomes and hepatocytes (Table 1). *In vivo* intravenous (iv) dosing at 1 mg/kg in Sprague Dawley rats confirmed a moderate plasma clearance and revealed a moderate volume of distribution and short terminal half-life (Table 1).

The favorable physicochemical parameters of **1** translated into high apparent permeability in Caco-2 cells with a low efflux ratio (Table 1). When administered orally to Sprague Dawley rats at 5 mg/kg in polyethylene glycol (PEG) 200/H<sub>2</sub>O (60/40; v/v), high plasma exposure ( $C_{max}$  = 1269 ng/mL and  $AUC_{0-inf}$  = 2588 ng·h/mL) was obtained for **1** with a 50% oral bioavailability (Table 1). The hit series did not show marked inhibition of either cytochrome P450 (CYP) or human ether-à-go-go-related gene (hERG).

At the start of our investigations, the presence of two methoxy groups in the 9 and 10 positions of the isoquinoline moiety raised some concerns, as such groups might play the role of the catechol ether structural motif common to most of the phosphodiesterase 4 (PDE4A) inhibitors<sup>21,22</sup> and introduce a PDE4A inhibitory component to the hit series already reported for 9 and 10 substituted dialkoxy analogues of pyrimido[6,1-*a*]isoquinolin-4-ones.<sup>23</sup>

PDE4 inhibitors possess a broad range of anti-inflammatory effects but have pronounced nausea and emesis side effects. As the aim of this project was to generate selective antagonists allowing us to unequivocally assess the therapeutic potential of GPR84, we wanted to show less than 50% inhibition over PDE4A at 10  $\mu$ M. PDE4A inhibitory activity of **1** was confirmed ( $IC_{50}$  = 553 nM; Table 1). This led us to implement a PDE4A biochemical assay to assess the inhibitory activity of

Table 1. Properties of Hit Compound 1<sup>a</sup>

1	
	2-(benzylamino)-9,10-dimethoxy-6,7-dihydro-4H-pyrimido[6,1-c]isoquinolin-4-one
	MW/XlogP3/PSA 363.4/2.4/63.2
hGPR84 GTPγS IC <sub>50</sub> (nM)	735
PDE4A IC <sub>50</sub> (nM)	553
aqueous solubility 2% DMSO (μg/mL)	>73/24
pH 3/pH 7.4	
liver microsomal stability	
CL <sub>int</sub> MIC scaled (L h <sup>-1</sup> kg <sup>-1</sup> )	mouse: 10.4 (n = 2) human: 1.9 (n = 2)
hepatocyte stability	
CL <sub>int</sub> HEP scaled (L h <sup>-1</sup> kg <sup>-1</sup> )	mouse: 10.6 (n = 2) human: 1 (n = 2)
intestinal permeability Caco-2 cells	
P <sub>app</sub> A <sub>2</sub> B (10 <sup>-6</sup> cm/s)/ER	15/2.0 (n = 2)
hCYP inhibition	
% inhibition at 10 μM	<33 with CYP1A2, CYP2C19, CYP2C9, CYP2D6, CYP3A4 (midazolam and testosterone)
rat PK 5 mg/kg po	
C <sub>max</sub> (ng/mL)	1269
AUC <sub>0–inf</sub> (ng·h/mL)	2588
F (%)	50
rat PK 1 mg/kg iv	
T <sub>1/2</sub> (h)	0.89
CL (L h <sup>-1</sup> kg <sup>-1</sup> ); CL (% LBF)	1.06; 21.6
V <sub>ss</sub> (L/kg)	1.27

<sup>a</sup>Abbreviations: AUC<sub>0–inf</sub>, area under curve (from time 0 to infinity); CL<sub>int</sub>, intrinsic clearance; C<sub>max</sub>, maximum plasma concentration; DMSO, dimethyl sulfoxide; ER, efflux ratio; hCYP, human cytochrome P450; F, oral bioavailability; GTPγS, guanosine 5'-O-[γ-thio]triphosphate; HEP, hepatocyte; hGPR84, human G-protein-coupled receptor 84; IC<sub>50</sub>, half maximal inhibitory concentration; iv, intravenous; LBF, liver blood flow; MIC, microsomal; MW, molecular weight; P<sub>app</sub> A<sub>2</sub>B, apparent permeability from apical to basal chambers; PDE4A, phosphodiesterase 4; PK, pharmacokinetics; po, per os; PSA, polar surface area; T<sub>1/2</sub>, half-life; V<sub>ss</sub>, apparent volume of distribution at steady state.

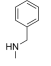
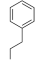
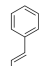
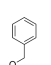
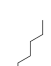
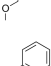

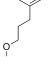
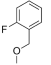
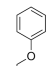
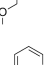
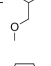
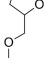
the compounds and gain SAR (structure–activity relationship) understanding to remove this residual PDE4A activity.

Initial SAR investigations focused on modifications of the benzyl amine moiety. Potency was abolished by either replacement of the nitrogen atom by a carbon atom (**2**) or introduction of a carbon–carbon double bond in place of the amino-methyl linker (**3**) (Table 2). A more favorable replacement was identified with the introduction of an oxygen atom, leading to an encouraging 5-fold increase in potency (**4**), compared with **1** (Table 2). We decided to consolidate the investigations with the oxygen atom in place.

Improved potency (IC<sub>50</sub> = 21 nM, Table 2) was observed with the introduction of an aliphatic chain that is common to the MCFA endogenous ligands (**5**), although solubility was drastically reduced by the lipophilic side chain (aqueous solubility [ASOL] pH 7.4 = 3 μg/mL).

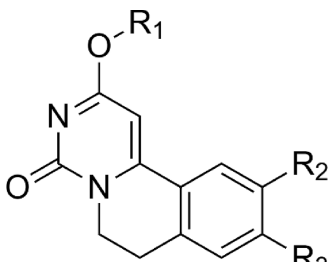
Various lipophilic spacers were introduced (**6** and **7**) and showed decreased potency compared with **4** (Table 2). With

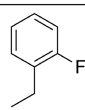
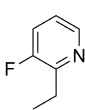
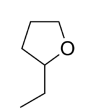
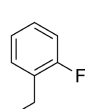
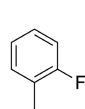
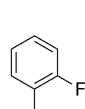
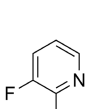
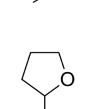
Table 2. hGPR84 GTPγS, PDE4A, Human Neutrophil Migration, and Solubility Profiles of 1 Derivatives<sup>a</sup>

Compd	R	hGPR84GT			
		PyS (IC <sub>50</sub> nM)	PDE4A (IC <sub>50</sub> nM)	Hum neutro (IC <sub>50</sub> nM)	ASOL pH 7.4 (μg/mL)
1		735	553	-	24
2		>10000	-	-	-
3		>10000	-	-	-
4		157	-	-	-
5		21	-	-	3.0
6		808	-	-	-
7		>10000	-	-	3
8		252	372	-	26
9		63	2115	128	26
10		350	1088	-	19
11		383	2165	-	72
12		> 10000	-	-	-
13		8	586	-	18

<sup>a</sup>Abbreviations: ASOL, aqueous solubility; Cap, capric acid; Compd, compound; hGTPγS, human guanosine 5'-O-[γ-thio]triphosphate; Hum neutro, human neutrophil migration assay; IC<sub>50</sub>, half maximal inhibitory concentration; IP1, inositol monophosphate; PDE4A, phosphodiesterase 4.

this ether linkage in place, introduction of a fluorine in the ortho position (**8**) had limited impact on potency, compared with **4**. Further assessment of PDE4A inhibitory activity

Table 3. hGTP $\gamma$ S, PDE4A, and Mouse Liver Microsomal Stability of Substructural Derivatives<sup>a</sup>


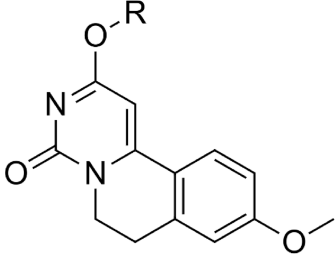
Compd	R <sub>1</sub>	R <sub>2</sub>	R <sub>3</sub>	hGPR84		Mouse LMS
				GTP $\gamma$ S (IC <sub>50</sub> nM)	PDE4A (IC <sub>50</sub> nM)	CL <sub>int</sub> scaled (L h <sup>-1</sup> kg <sup>-1</sup> )
8		OMe	OMe	252	372	40.2
10		OMe	OMe	350	1088	6.1
11		OMe	OMe	383	2165	10.5
14		H	H	1950	>10000	82.0
15		H	OMe	1143	>10000	89.2
16		OMe	H	8470	>10000	118
17		H	OMe	595	>10000	29.2
18		H	OMe	3073	-	129

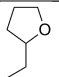
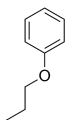
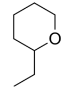
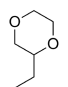
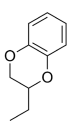
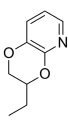
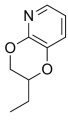
<sup>a</sup>Abbreviations: Compd, compound; CL<sub>int</sub>, intrinsic clearance; hGTP $\gamma$ S, human guanosine 5'-O-[ $\gamma$ -thio]triphosphate; IC<sub>50</sub>, half maximal inhibitory concentration; LMS, liver microsomal stability; Me, methyl group; PDE4A, phosphodiesterase 4.

showed no selectivity improvement. Moreover, **8** showed decreased metabolic stability in mouse microsomes (Table 3), compared with **1**.

We probed the scope of polarity introduction which, if tolerated, could be beneficial for further improvement of metabolic stability. The addition of an ethylene glycol spacer

(**9**) restored good potency (IC<sub>50</sub> = 63 nM) and gave a 150-fold increase compared with the match paired analogue (**7**) (Table 2). This disparity indicated a strong contribution from the oxygen atom introduced, possibly resulting from an H-bond interaction. Compound **9** showed a reduced inhibitory activity on PDE4A (Table 2), leading to a 30-fold ratio selectivity.

Table 4. hGTP $\gamma$ S, PDE4A, Liver Microsomal Stability, Hepatocyte Stability, PPB, and XlogP3 Profiles for Substructural Derivatives<sup>a</sup>


Compd	R	hGPR84	PDE4A	Liver microsomal		Hepatocyte stability		PPB	XlogP3
		GTP $\gamma$ S (IC <sub>50</sub> nM)	(IC <sub>50</sub> $\mu$ M)	stability	CL <sub>int</sub> MIC scaled (L h <sup>-1</sup> kg <sup>-1</sup> )	CL <sub>int</sub> HEP scaled (L h <sup>-1</sup> kg <sup>-1</sup> )	(% bound)		
18		3073		M: 129 H: 2.0		M: 38.8 H: 1.4	-	1.9	
19		156	>10	M: 64.9 H: 3.8		M: 34.9 H: 2.5	M: 98.9 R: 78.2	3.2	
20		608		M: 27.8 H: 1.3		M: 34.5 H: 1.5	-	2.3	
21		431		M: 10.4 R: <1.4 H: <0.9		M: 15.7 H: <0.7	M: 61.1 R: 71.5 H: 77.7	1.1	
22		50		M: 31.9 R: 36.9 H: 4.6		M: 22.5 H: 5.4	M: 99.0 R: 99.6 H: 99.8	3.0	
23		873		M: <3.0 H: <0.9		M: 11.3 H: 1.6	M: 97.0 H: 99.1	2.2	
24		22		M: 21.6 R: 9.1 H: 2.1		M: 10.9 H: 0.8	M: 91.3 R: 97.9 H: 97.3	2.2	

<sup>a</sup>Abbreviations: CL<sub>int</sub>, intrinsic clearance; H, human; HEP, hepatocyte; hGTP $\gamma$ S, human guanosine 5'-O-[ $\gamma$ -thio]triphosphate; IC<sub>50</sub>, half maximal inhibitory concentration; M, mouse; MIC, microsomal; PPB, plasma protein binding; PDE4A, phosphodiesterase 4; R, rat.

Internal investigations identified that GPR84 agonists such as embelin, DIM, and sodium decanoate were able to induce human neutrophil migration. GPR84 antagonists were able to specifically block neutrophil chemotaxis induced by GPR84 agonists (Supplemental Figure 4). The embelin-induced neutrophil chemotaxis assay was used as an inflammatory disease relevant cell assay to determine the inhibitory activity of our GPR84 antagonists. Assessment of **9** showed a good translation of the antagonist effect on a target based GTP $\gamma$ S

assay toward the human neutrophil migration assay (IC<sub>50</sub> = 128 nM; Table 2). Comparing the matched pairs **10** and **8** showed that the introduction of one nitrogen atom had only a moderate impact on potency; however, a positive impact was observed on metabolic stability (Table 3) and its selectivity toward PDE4A (IC<sub>50</sub> = 1088; Table 2).

Replacement of the phenyl ring with a more polar tetrahydrofuran was tolerated for the 2-substituted heterocycle (**11**) and found inactive for the 3-substituted analogue (**12**)

Table 5. hGTP $\gamma$ S, XlogP3, Metabolic Stability, and Permeability Profiles of 25, 26, and 27<sup>a</sup>

Compd	R <sub>1</sub>	R <sub>2</sub>	hGPR84		Liver microsomal stability					Caco-2 cells		
			GTP $\gamma$ S	XlogP3	CL <sub>int</sub> MIC scaled (L h <sup>-1</sup> kg <sup>-1</sup> )					P <sub>app</sub> A <sub>2</sub> B (x10 <sup>-6</sup> cm/sec)		
			(IC <sub>50</sub> nM)		Mouse	Rat	Dog	Monkey	Human	/ ER		
25			274	2.57								
26			212	2.42	9.05	6.3	10	11.6	5.2		1.3	
27			0.6	3.48								

<sup>a</sup>Abbreviations: CL<sub>int</sub>, intrinsic clearance; Compd, compound; ER, efflux ratio; hGTP $\gamma$ S, human guanosine 5'-O-[ $\gamma$ -thio]triphosphate; IC<sub>50</sub>, half maximal inhibitory concentration; MIC, minimum inhibitory concentration; P<sub>app</sub> A<sub>2</sub>B, apparent permeability from apical to basal chambers.

(Table 2). This result is associated with the favorable impact observed on potency with the oxygen introduction (9) and may be indicative of a specific interaction of GPR84 with an oxygen atom in this position. In addition to increased potency, the position of oxygen in 11 improved selectivity against PDE4A (IC<sub>50</sub> = 2165 nM; Table 2) and solubility (9, ASOL pH 7.4 = 26  $\mu$ g/mL and 11, ASOL pH 7.4 = 72  $\mu$ g/mL). The potency of 9, in the human neutrophil assay (IC<sub>50</sub> = 128 nM; Table 2), prompted investigation into the tolerance of further polarity. Replacement of the phenyl ring of 9 with a 2-pyridyl ring increased both the potency toward the target and the selectivity ratio over PDE4A (13, GTP $\gamma$ S IC<sub>50</sub> = 8 nM and selectivity ratio = 73).

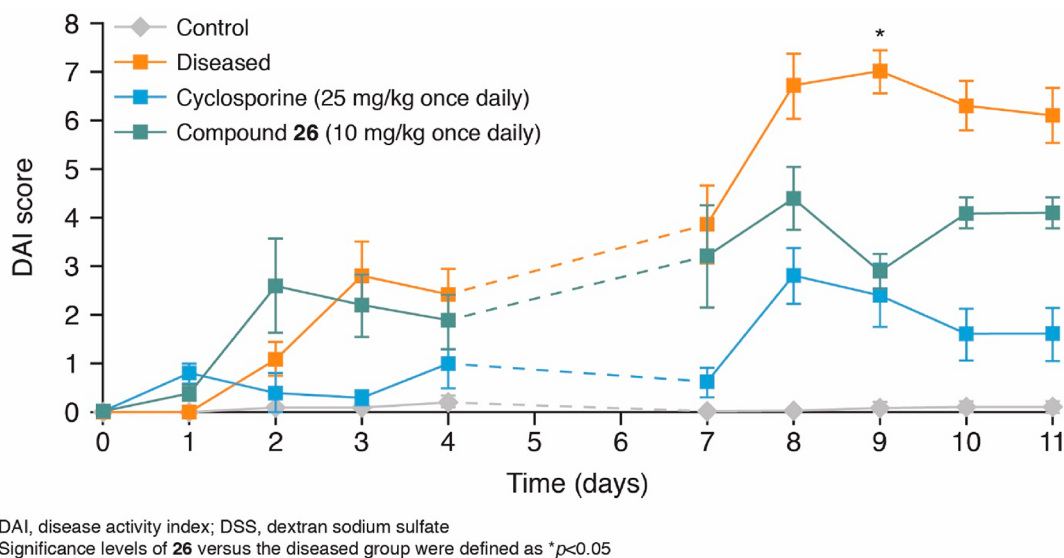
Sequence differences between human and mouse GPR84 (mouse GPR84 shares 85% with its human ortholog at the amino acid level) prompted us to assess activity of the hit series on mouse GPR84 receptor assays. At this stage of investigation, no cell line stably overexpressing the mouse receptor for the GTP $\gamma$ S assay was available. An assay measuring inositol monophosphate (IP1) using transiently transfected HEK293 cells with either the human or mouse recombinant GPR84 and a variant of a chimeric Gq protein was developed to allow direct comparison on mouse and human receptor under similar assay conditions. We confirmed the high inhibitory activity of 13 in the IP1-based hGPR84 assay (hGPR84 IP1 IC<sub>50</sub> = 11 nM) and observed an approximate 60-fold reduction in the IP1-based mouse GPR84 assay (mGPR84 IP1 IC<sub>50</sub> = 636 nM).

Initial investigations demonstrated that a high potency in the nanomolar range could be reached in the human GTP $\gamma$ S assay,

which translated into potent inhibition of human neutrophil migration. Further optimization comprised the consolidation of the attractive profile of the series, with the aim to improve the selectivity ratio by producing a compound that was inactive in the PDE4A assay or had at least a 100-fold selectivity.

The presence of the catechol ether moiety in known potent inhibitors of PDE4A suggested a key role for this functional group in the enzyme pharmacophore, prompting further investigation of the impact of modifications in this region. The presence of the two methoxy substituents was found to be crucial to PDE4A activity but not mandatory for maintaining GPR84 inhibitory activity, as illustrated with the unsubstituted analogue 14 (Table 3). Removal of either methoxy group markedly decreased PDE4A activity for the corresponding analogues (15 and 16; Table 3). Of particular interest were the 9-methoxy substituted analogues, which showed a less than 10-fold loss of GPR84 activity in three matched pairs (17 and 10; 18 and 11; 15 and 8; Table 3). The favorable selectivity trend was found to be well conserved when applied to the 2-fluoropyridine analogue (17 and 10; Table 3). Despite decreased metabolic stability in mouse liver microsomes observed for the 9-substituted analogue 17 compared with the dimethoxy substituted analogue 10 (Table 3), the gain in selectivity and the attractiveness of the undocumented 9-methoxy derivatives led us to continue in this direction.

Introduction of the phenoxyethyl group (19) led to a 20-fold increase in potency compared with the moderately potent starting point 18 (Table 4), a marked improvement from the previous 6-fold increase in potency for the dimethoxy substituted matched pair analogues 11 and 9. Additionally,



**Figure 2.** Disease activity index score in a mouse DSS-induced chronic colitis model. Diseased mice were administered with 4% DSS in drinking water for 4 days, followed by 3 days of regular drinking water and a new cycle of DSS. In addition they were orally administered **26** at 10 mg/kg once daily (qd), cyclosporine at 25 mg/kg qd (positive control), or vehicle for 11 consecutive days. Control mice were administered water alone as a negative control. Data are the mean  $\pm$  SEM. No scores were measured on days 5 and 6.

**19** achieved good selectivity with an inhibitory activity above 10  $\mu$ M in the PDE4A assay (Table 4). Within the chemical series, the preliminary results observed from liver microsomal stability data and the lipophilicity of the compounds seemed to point toward a favorable XlogP3 threshold below 3. Subsequent SAR optimization aimed to keep lipophilicity with XlogP3 below 3, retain the key  $\beta$ -oxygen, and determine the most suitable moieties for demonstrating a good metabolic profile while maintaining acceptable potency and selectivity.

Replacement of the 2-tetrahydrofuryl with the homologous tetrahydro-2H-pyranyl moiety improved potency (**20**; Table 4) with a moderate increase in lipophilicity. However, a significant reduction in lipophilicity was achieved with the introduction of the 1,4-dioxane (**21**) with similar potency compared with **20** and improved metabolic stability in mouse and human liver microsomes and hepatocytes. The attractive absorption, distribution, metabolism, and excretion (ADME) profile obtained by introduction of the dioxane moiety prompted attempts to mitigate the associated reduced potency by adding moderate lipophilicity with fused heterocycles on the dioxane. This was achieved through fusion of a phenyl ring to produce **22** with increased potency ( $IC_{50} = 50$  nM; Table 4) but with severely reduced stability in mouse, rat, and human liver microsomes.

To reduce the lipophilicity, a 2-pyridyl ring was fused to the dioxane to give **23**. However, the introduction of the nitrogen in the ortho position of the key  $\beta$ -oxygen resulted in reduced potency compared with **22**. Introducing the nitrogen to the ortho position of the other oxygen in the dioxane ring had a positive impact on potency (**24**) but was accompanied by a high intrinsic liver microsomal clearance in mice (Table 4). Assessment of the metabolic stability of compounds **18–24** in hepatocytes showed a good correlation of intrinsic clearance between liver microsomes and both mouse and human hepatocytes, indicating a major contribution in phase I metabolism (Table 4).

With the high potency of **24**, further optimization investigations focused on modifications of the 9 position

with opportunistic introduction in one step of diverse and exotic commercially available moieties (Table 5). Assessment of the tolerability of this region to substantial modulation was investigated through the introduction of a negatively charged chain and a very bulky moiety. Interestingly, substitution of the methyl group with an acetic acid group from the potent compound **22** led only to a moderate 5-fold decrease in potency (**25**; Table 5). Replacement of the methoxy group with 2-cyanophenyl (**26**) was neutral ( $IC_{50} = 212$  nM; Table 5) when compared with **21**. The compound was unstable in dog, monkey, and human liver microsomes, but moderate clearance was observed in rodents. Furthermore, **26** demonstrated good permeability in Caco-2 cells with low efflux and high systemic exposure in rat at 5 mg/kg ( $AUC_{0-2}$  of 2645 ng·h/mL [6.37  $\mu$ M·h] following oral dosing in PEG200/water [60/40; v/v]) providing an interesting opportunity to evaluate the capability of the lead series to modulate inflammatory bowel disease (IBD).

To assess *in vivo* efficacy, **26** was studied in a mouse chronic dextran sodium sulfate (DSS)-induced colitis model, a well-validated model for IBD.<sup>24,25</sup> The DSS treatment significantly increased the disease activity index (DAI) score (sum of scores for weight loss, stool consistency, and fecal blood) reflecting active colitis. As expected, once-daily treatment with the positive control cyclosporine (administered at 25 mg/kg, once daily [qd]) diminished the DAI score in diseased mice. Once-daily treatment with **26** at 10 mg/kg qd reduced the DAI score at 8–11 days ( $p < 0.05$  at day 9 versus diseased mice) (Figure 2). Encouraged by these *in vivo* data, subsequent optimization of the lead series was aimed at improving *in vivo* potency and metabolic stability in dog and human.

A 33-fold gain in potency was achieved by the addition of a bulky phenylpro-2-yn-1-ol moiety to the highly potent compound **24** to produce **27** with a subnanomolar potency on GPR84 ( $IC_{50} = 0.6$  nM; Table 5). This result confirmed the option of replacing the oxygen linker at the 9 position with a carbon atom, as with **26**. These additions, of both the negatively charged chain and bulky moiety, indicated a broad

Table 6. hGTP $\gamma$ S, XlogP3, PDE4A, IP1, Liver Microsomal Stability, and Human Neutrophil Migration Profiles of Substructural Derivatives<sup>a</sup>

Compd	R	hGPR84		PDE4A (IC <sub>50</sub> nM)	IP1 mouse/ human (Cap: IC <sub>50</sub> nM)	LMS CL <sub>int</sub> MIC scaled (L/h/kg)	Hum neutro (IC <sub>50</sub> nM)
		GTP $\gamma$ S (IC <sub>50</sub> nM)	XlogP3				
28		466	1.9	-	-	-	-
29		107	2.0	-	-	-	-
30		84	1.7	-	-	-	-
31		26	2.0	-	-	-	-
32		8	2.3	-	M: 39 H: 6	M: 31.0 H: 1.5	-
33		25	2.3	-	-	R: 15.3 M: 26.2	-
34		22	2.8	-	-	M: 26.0 H: 5.3	-
35		55	2.4	Not active	-	M: 9.7 R: 1.4 H: 2.2	17

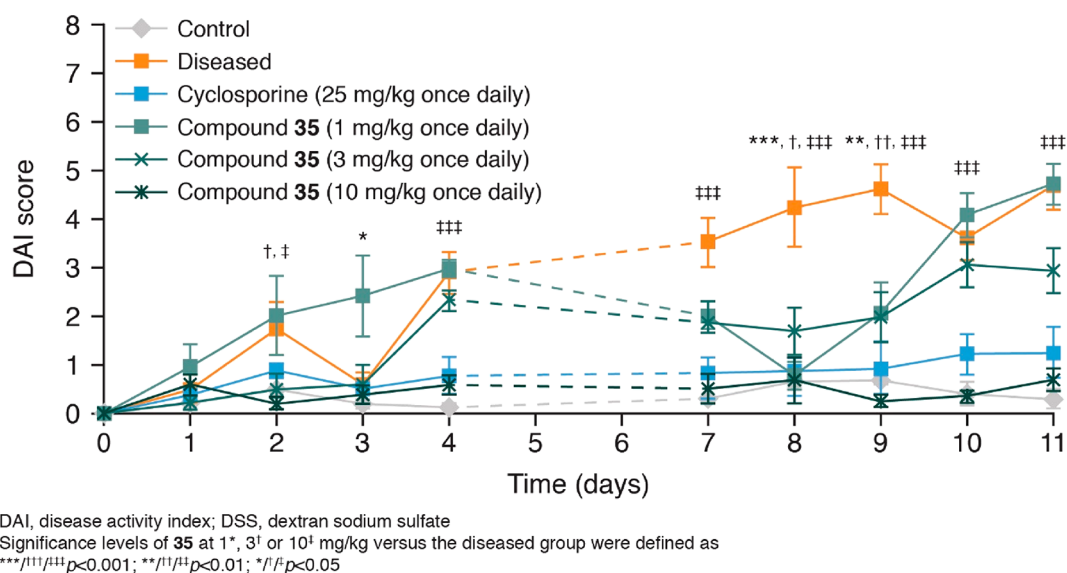
<sup>a</sup>Abbreviations: CL<sub>int</sub>, intrinsic clearance; Compd, compound; D, dog; H, human; hGTP $\gamma$ S, human guanosine 5'-O-[ $\gamma$ -thio]triphosphate; Hum neutro, human neutrophil migration; IC<sub>50</sub>, half maximal inhibitory concentration; IP1, inositol monophosphate; LMS, liver microsomal stability; M, mouse; MIC, microsomal; PDE4A, phosphodiesterase; R, rat.

SAR tolerance in this region of the molecule. Further modification of this region was pursued with the aim of maintaining overall lipophilicity below the defined threshold for the series while benefiting from a gain in potency.

The high potency of **27** was associated with increased lipophilicity (Table 5), so further modifications aimed to

achieve a good balance of these properties. The moderately potent **21** (Table 4) was selected as a starting compound as it afforded a 2 log margin for lipophilicity and required only an approximate 10-fold gain in potency to produce an attractive target molecule. Removal of the 9-methoxy substituent (**28**; Table 6) had a minor impact on the lipophilicity and the





**Figure 3.** Disease activity index score in a mouse DSS-induced chronic colitis model. Diseased mice were administered with 4% DSS in drinking water for 4 days, followed by 3 days of regular drinking water and a new cycle of DSS. In addition they were orally administered **35** at 1\*, 3<sup>†</sup> or 10<sup>†</sup> mg/kg qd, cyclosporine at 25 mg/kg qd (positive control), or vehicle, for 11 consecutive days. Control mice were administered water alone as a negative control. Data are the mean  $\pm$  SEM. No scores were measured on days 5 and 6.

inhibitory activity (Table 6). Introduction of groups with growing size to maintain lipophilicity in the targeted range improved the potency (29, 30, and 31; Table 6). Introduction of a 2 ethylpyridyl moiety maintained a moderate lipophilicity and gave a remarkable potency (32) in human GTP $\gamma$ S and IP1 assays and reduced orthology shift in the mouse IP1 assay. However, while the compound showed low clearance in human microsomes (intrinsic clearance ( $CL_{int}$ ) scaled of 1.5 L h<sup>-1</sup> kg<sup>-1</sup>), it was highly cleared in mouse liver microsomes ( $CL_{int}$  scaled of 31 L h<sup>-1</sup> kg<sup>-1</sup>) precluding further *in vivo* evaluation of the compound.

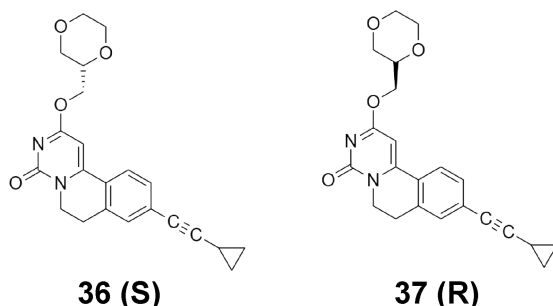
We decided to further exploit the initial path identified with compound 27 (Table 5). Starting from a decreased level of lipophilicity, due to the removal of the fused pyridyl moiety, the phenyl ring linked to the secondary alcohol was replaced with an isobutyl group limiting the lipophilicity at XlogP3 = 2.3. Compound 33 showed good potency ( $IC_{50}$  = 25 nM; Table 6); however, in spite of a moderate lipophilicity, the compound was found to be insufficiently stable in rat liver microsomes ( $CL_{int}$  scaled of 15.3 L h<sup>-1</sup> kg<sup>-1</sup>). Compound 34 was designed to remove the propargylic alcohol as a putative metabolite site and introduce a basic benzyl amine moiety. These modifications retained potency ( $IC_{50}$  = 22 nM; Table 6), but 34 showed elevated liver microsomal clearances in both mouse and human (in mouse,  $CL_{int}$  scaled of 26 L h<sup>-1</sup> kg<sup>-1</sup> and in human,  $CL_{int}$  scaled of 5.3 L h<sup>-1</sup> kg<sup>-1</sup>).

The addition of a simple cyclopropyl ring into the alkyne moiety maintained both acceptable lipophilicity and potency ( $IC_{50}$  = 55 nM; Table 6), and the resulting compound **35** was devoid of PDE4A activity. The high potency of the compound was confirmed in a human IP1 assay ( $IC_{50}$  = 2 nM) and was found to be 10-fold less potent in the same assay in mice ( $IC_{50}$  = 21 nM). In accordance with previous data, the high potency of **35** in GPR84 functional assays corresponded to high potency in human neutrophil migration assays ( $IC_{50}$  = 17; Table 6). A rat neutrophil migration assay was successfully developed and confirmed the high inhibitory activity of the compound ( $IC_{50}$  = 119 nM) and the shift in activity from

human to rodent. Additionally, **35** showed acceptable metabolic stability in human, rat, and mouse liver microsomes ( $CL_{int}$  scaled of 2.2, 1.4 and 9.7, respectively).

The attractive profile of **35**, with good potency in rat and human *in vitro* assays and improved metabolic stability in human liver microsomes, led to further *in vivo* studies. High plasma exposure was observed following oral administration at 5 mg/kg in rats with an  $AUC_{0-inf}$  of 10246 ng·h/mL and a  $C_{max}$  of 2423 ng/mL at 1.7 h. In a mouse DSS-induced chronic IBD model, once-daily treatment with **35** at 1, 3, or 10 mg/kg dose-dependently reduced the DAI score; **35** at 10 mg/kg was found to have similar efficacy as cyclosporine at 25 mg/kg, the positive control (Figure 3).

The attractive profile of the compound instigated efforts to isolate and characterize the two enantiomers of **35** (Table 7). When profiled in terms of ADME and biological assays, the two enantiomers (*S*) **36** and (*R*) **37** showed moderate differences favoring the (*S*) enantiomer **36** (Table 7). Compound **36** was approximately 5-fold more potent in human neutrophil migration assays (Table 7) but only slightly more potent in human GTP $\gamma$ S and rat and dog neutrophil migration assays (Table 7). Both enantiomers appeared stable in hepatocytes when incubated at 1  $\mu$ M, with a low predicted hepatic clearance for rat, mouse, dog, and human (Table 7). The two enantiomers did not show marked differences in binding to plasma protein when assessed in four different species in an *in vitro* equilibrium dialysis PPB assay (tested at 5  $\mu$ M) (Table 7). The assessment of the CYP inhibitory potential of the two enantiomers was markedly more favorable for **36**. The  $IC_{50}$  was determined using human liver microsomes with probe substrates for CYP1A2, 2C9, 2C19, 2D6, and 3A4 (Table 7). The  $IC_{50}$  value for **36** for each of the CYP isoenzymes was >33  $\mu$ M (Table 7), whereas the (*R*) enantiomer showed micromolar inhibition of the CYP2C9 isoform ( $IC_{50}$  = 1.85  $\mu$ M; Table 7) and moderate inhibition of CYP2C19 ( $IC_{50}$  = 18  $\mu$ M; Table 7). In addition, there was no evidence for time-dependent inhibition of CYP3A4 by **36** (human liver microsomes, midazolam, and testosterone used as

Table 7. Profiles of the Two Enantiomers of 35<sup>a</sup>


	36 (S)	37 (R)
hGPR84 (GTP $\gamma$ S IC <sub>50</sub> , nM)	54	102
human neutrophil assay (IC <sub>50</sub> , nM)	11	51
rat neutrophil assay (IC <sub>50</sub> , nM)	111	153
dog neutrophil assay (IC <sub>50</sub> , nM)	75	111
aqueous solubility 2% DMSO ( $\mu$ g/mL)		
pH 3/pH 7.4	113/113	113/113
thermodynamic solubility ( $\mu$ g/mL)		
pH 3/pH 7.4	12.6/7.75	17.6/9.49
liver microsomal stability 1 $\mu$ M		
CL <sub>int</sub> MIC scaled (L h <sup>-1</sup> kg <sup>-1</sup> )		
mouse	8.0	5.9
rat	4.0	4.97
dog	5.34	3.16
human	<1.16	0.962
hepatocyte stability 1 $\mu$ M		
T <sub>1/2</sub> (min)/CL <sub>int</sub> HEP scaled (L h <sup>-1</sup> kg <sup>-1</sup> )		
mouse	>200/ <4.37	>200/ <4.37
rat	>200/<2.0	>188/ <2.12
dog	>200/ <1.45	>151/ <1.92
human	>200/ <1.28	>200/ <1.28
intestinal permeability Caco-2 cells		
P <sub>app</sub> A <sub>2</sub> B ( $\times 10^{-6}$ cm/s)/ER	41.9/1.05	31.2/1.07
CYP inhibition HLM IC <sub>50</sub> ( $\mu$ M)		
1A2	>100	>100
2C19	>100	18.2
2D6	>100	31.6
2C9	34.6	1.85
3A4 mid	>50	>50
3A4 test	>50	>50
PPB % bound		
mouse	97.8	98.3
rat	97.7	96.3
human	97.2	94.1
dog	93.5	96.7

<sup>a</sup>Abbreviations: CL<sub>int</sub>, intrinsic clearance; CYP, cytochrome P450; DMSO, dimethyl sulfoxide; ER, efflux ratio; GTP $\gamma$ S, guanosine 5'-O-[ $\gamma$ -thio]triphosphate; HEP, hepatocyte; HLM, human liver microsome; IC<sub>50</sub>, half maximal inhibitory concentration; IP1, inositol monophosphate; MIC, microsomal; P<sub>app</sub> A<sub>2</sub>B, apparent permeability from apical to basal chambers; PPB, plasma protein binding.

probe substrates to assess remaining enzyme activity) and the IC<sub>50</sub> was >50  $\mu$ M, both with and without preincubation.

The pharmacokinetic profile (PK) of 36 was assessed in three species (mouse, rat, and dog) after an iv administration at 1 mg/kg (in mouse) or 0.5 mg/kg (in rat and dog) and an oral administration in fasted animals at 5 mg/kg (in mouse) or 2.5 mg/kg (in rat and dog). PEG200/NaCl 0.9% (60/40; v/v) was used as formulation for the iv route and PEG200/water (60/40; v/v) for the po route. A high oral exposure was

obtained in all three species (Table 8), giving a bioavailability of 100%. A high total clearance was observed in dogs but did not preclude its progression owing to acceptable clearances in other species. The use of the recently introduced unbound clearance parameter shows that this is due to the lower PPB in dog (93.5% of binding) compared with mouse, rat, and human, leading to a lower unbound clearance (CL<sub>unb</sub> = 18.5). The volume of distribution was low in mice and high in dogs.

In competition studies, 36 was found to block agonist effects of both modulators considered as orthosteric ligands, such as C10 and embelin, and allosteric ligands, such as PSB-16671 (Figures 1 and 4A). In parallel to the progression of 36, additional potent compounds with modified substitutions in position 9 and different side chains in the northern region of the compound were identified. Compound 38, with a phenethyl chain in position 9 and a 2-ethoxypyrazine moiety in the northern region (Figure 4B), reached a high potency level in the hGTP $\gamma$ S assay (IC<sub>50</sub> = 5 nM). In addition to being one of the most potent analogues in the GTP $\gamma$ S assay, the straightforward synthetic introduction of a tritium atom into the molecule from the corresponding 3-chlorophenethyl derivative guided the selection of 38 as a target for generating a radiolabeled ligand ([<sup>3</sup>H]38 was prepared by Quotient Bioresearch). Compound 36 competed well with its analogue [<sup>3</sup>H]38 with a pK<sub>i</sub> of 7.52. Increasing concentrations of C10 were unable to displace the [<sup>3</sup>H]38 ligand, suggesting an allosteric binding site for the GPR84 antagonists (Figure 4C). In the same competition experiment, PSB-16671, an allosteric agonist from the DIM series, showed only moderate displacement at a very high dose (Figure 4C). In a Schild experiment, further characterization of the interaction between the two ligands showed 36 to act dose-dependently as a noncompetitive and reversible blocker of PSB-16671, with a decreased maximum effect rather than markedly increasing the half maximal effective concentration (EC<sub>50</sub>) (Figure 4D). These results, combined with previous studies showing that [<sup>3</sup>H]38 binding was not affected by mutation of key residue Arg172,<sup>26</sup> indicate that 36 acts as a negative allosteric modulator of the known GPR84 agonists.

In a mouse DSS-induced chronic IBD model, once-daily treatment with 36 at 3 or 10 mg/kg reduced the DAI score (Figure 5A). In the colon, compound 36 also reduced neutrophil infiltration induced by DSS, a pharmacodynamics marker in relation to *in vitro* neutrophil chemotaxis activity (Figure 5B). The pharmacodynamics marker was reversed by 36 at 3 mg/kg and 10 mg/kg, with a similar dose effect to DAI. This provides a mechanistic insight, clearly indicating the capacity of 36 to reduce neutrophil migration toward the inflamed colonic tissue. This activity was associated with a C<sub>max</sub> of 1837 ng/mL and an exposure level (AUC<sub>0–24h</sub>) of 5556 ng·h/mL (Table 9).

Compound 36 was tested in three independent mouse DSS-induced chronic IBD studies at 1, 3, or 10 mg/kg to confirm the efficacy and to define the minimal efficacious dose (MED). The dose of 1 mg/kg dose was inactive; however the dose of 3 mg/kg was constantly found active in all three studies and thus was considered as the MED.

Compound 36 was further profiled in a diverse set of selectivity assays. Compound 36 was fully selective over close homologs GPR43 (FFA2R) and GPR41 (FFA3R) (no inhibition up to 10  $\mu$ M in [Ca<sup>2+</sup>]<sub>i</sub> flux assay) and >100-fold selective over 123 other GPCRs on a Millipore GPCR Profiler panel. Compound 36 was remarkably selective over a kinase

Table 8. Pharmacokinetic Parameters of 36 in Different Species<sup>a</sup>

		mouse		rat		dog	
		1 mg/kg iv (n = 3)	5 mg/kg po (n = 3)	0.5 mg/kg iv (n = 3)	2.5 mg/kg po (n = 3)	0.5 mg/kg iv (n = 3)	2.5 mg/kg po (n = 3)
C <sub>0</sub> or C <sub>max</sub>	(ng/mL)	1227	4593	395	1164	NC	558
T <sub>max</sub>	(h)		0.5		1.5		0.5
AUC <sub>(0–24h)</sub>	(ng·h/mL)	1054	15349	710	4469	410	2232
CL	(L h <sup>-1</sup> kg <sup>-1</sup> )/(% LBF)	0.9/11		0.7/14		1.2/48	
CL <sub>unb</sub>	(L h <sup>-1</sup> kg <sup>-1</sup> )	40.9		30.4		18.5	
V <sub>ss</sub>	(L/kg)	0.6		1.2		2.0	
t <sub>1/2</sub>	(h)	0.6	1.9	1.0	1.3	1.4	2.0
F	(%)		>100		>100		>100

<sup>a</sup>Abbreviations: AUC, area under curve; CL, clearance; CL<sub>unb</sub>, clearance unbound calculated using PPB data (Table 7); C<sub>max</sub>, maximum plasma concentration; C<sub>0</sub>, concentration extrapolated at T<sub>0</sub> after a bolus iv dose; F, bioavailability; LBF, liver blood flow; t<sub>1/2</sub>, half-life; T<sub>max</sub>, time at C<sub>max</sub>; V<sub>ss</sub>, volume of distribution.

panel, displaying only weak inhibitory activity against maternal embryonic leucine zipper kinase (MELK; 57% inhibition at a concentration of 10 μM) out of a selection of 152 kinases (Reaction Biology, Malvern, PA, USA); this inhibitory activity was not considered to be clinically relevant. Similar high selectivity was also observed against a diverse panel of 67 enzymes focusing mostly on ion channels and transporters. Compound 36 was considered to present a low cardiovascular risk due to the minimal impact observed on the amplitude of the IKr current in the *in vitro* hERG manual patch clamp assay and the lack of effect on hemodynamic and electrocardiographic parameters in telemetered monkeys. Compound 36 was assessed in the full Ames test, up to concentrations of 5000 μg/plate, in the presence and absence of S9 fraction, leading to the conclusion that 36 is not mutagenic in the *Salmonella typhimurium* reverse mutation assay and in the *Escherichia coli* reverse mutation assay. Compound 36 did not have any genotoxic effect *in vitro* in the mouse lymphoma assay or *in vivo* in the bone marrow micronucleus test in rats. Compound 36 did not show any teratogenic or embryotoxic effects in rats, up to the highest tolerated maternal dose of 50 mg kg<sup>-1</sup> day<sup>-1</sup>. In addition, no phototoxic effects with 36 have been observed *in vivo* in rats and mice.

## CHEMISTRY

**GLPG1205 Synthesis.** GLPG1205 (36) was synthesized in nine linear steps that all proceeded with yields higher than 70% and involved readily available starting material (Scheme 1).

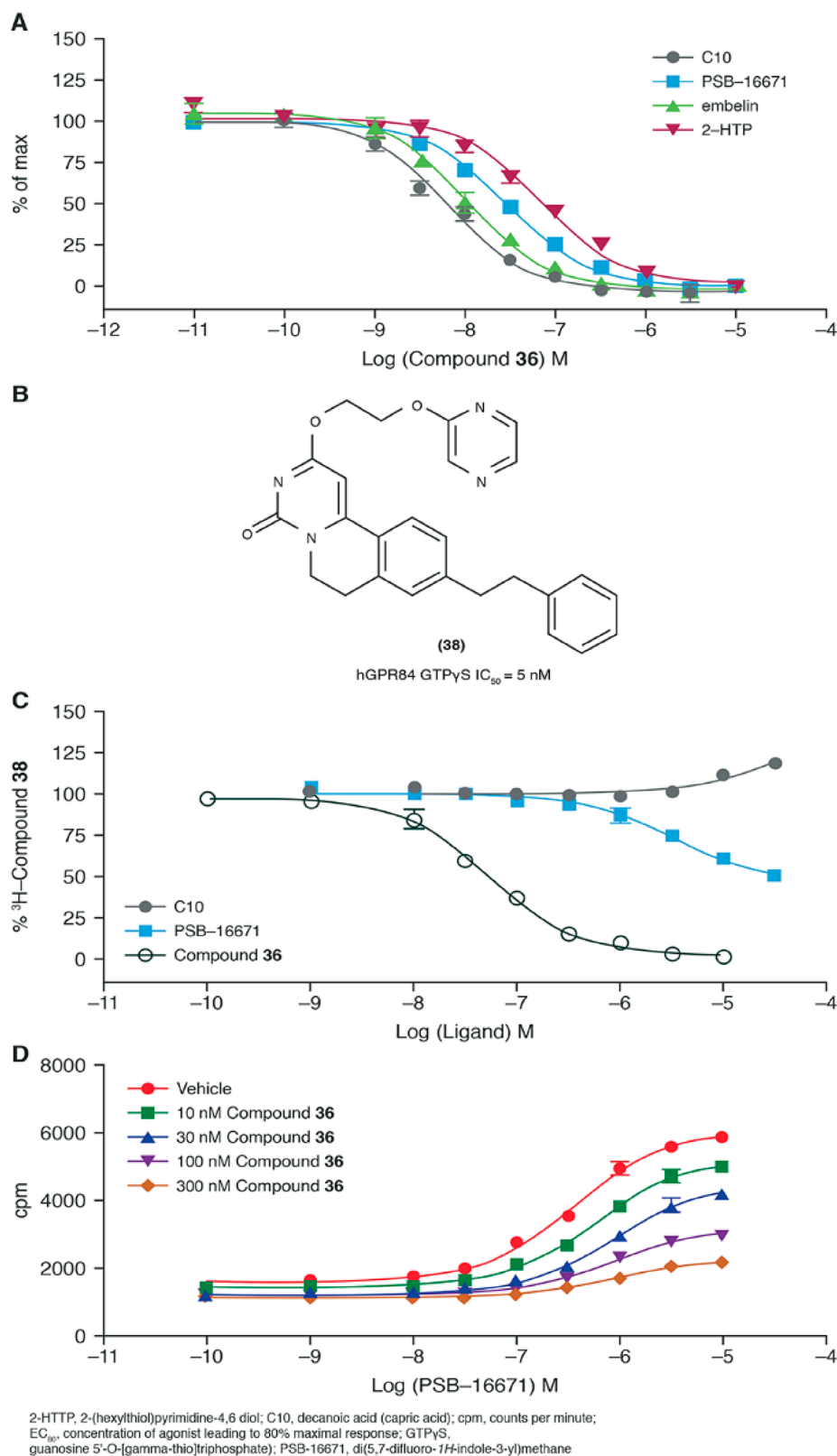
Starting from 3-methoxyphenethylamine, refluxing urea in acetic acid overnight led to the urea analogue. Demethylation was carried out upon overnight reflux with hydrogen bromide to lead to the corresponding phenol derivative which was further protected by introduction of an allyl group. Condensation with diethyl malonate afforded the hexahydropyrimidine-2,4,6-trione which underwent regioselective cyclization reaction with treatment with POCl<sub>3</sub>. Subsequent O-alkylation with commercially available or easily prepared (R)-(1,4-dioxan-2-yl)methanol<sup>27</sup> followed by deprotection of the allyl group led to the phenol intermediate. The phenol intermediate was converted into the corresponding triflate for further use in Sonogashira coupling reaction with ethynylcyclopropane, providing GLPG1205. The purity of all compounds was determined by liquid chromatography–mass spectrometry (LCMS) and <sup>1</sup>H NMR. Minor adaptations of this synthetic route afforded 9,10-dimethoxy derivatives starting from 3,4-dimethoxyphenethylamine.

## CONCLUSION

The progression of the commercially available hit compound 1 to the clinical candidate 36 was achieved by structure optimization to improve potency (GTPγS assay), metabolic stability, lipophilicity, and selectivity against PDE4A. In a mouse DSS-induced chronic IBD model, treatment with 36 reduced both the DAI score and neutrophil infiltration at oral doses of 3 and 10 mg/kg qd, with an efficacy similar to the positive control compound sulfasalazine. A phase I first-in-human study<sup>28</sup> and a phase IIa study in IBD (ulcerative colitis; NCT02337608)<sup>29</sup> confirmed favorable PK, safety, and tolerability profiles for 36, but the compound failed to meet the primary efficacy end point in the latter, and as GLPG1205 is the first in class GPR84 antagonist tested in clinical study, additional translational studies would contribute to the further understanding of results.<sup>29</sup> The biology of GPR84 has been further investigated and a potential role in fibrosis described in different organs including the kidney<sup>16</sup> and liver.<sup>30</sup> Moreover, GLPG1205 (36) has demonstrated reduced lung fibrosis in two mouse models in a therapeutic setting.<sup>31</sup> GLPG1205 (36) is currently being evaluated in a phase II study in patients with idiopathic pulmonary fibrosis. Additional safety, pharmacological, PK, and clinical data will be reported in due course.

## EXPERIMENTAL SECTION

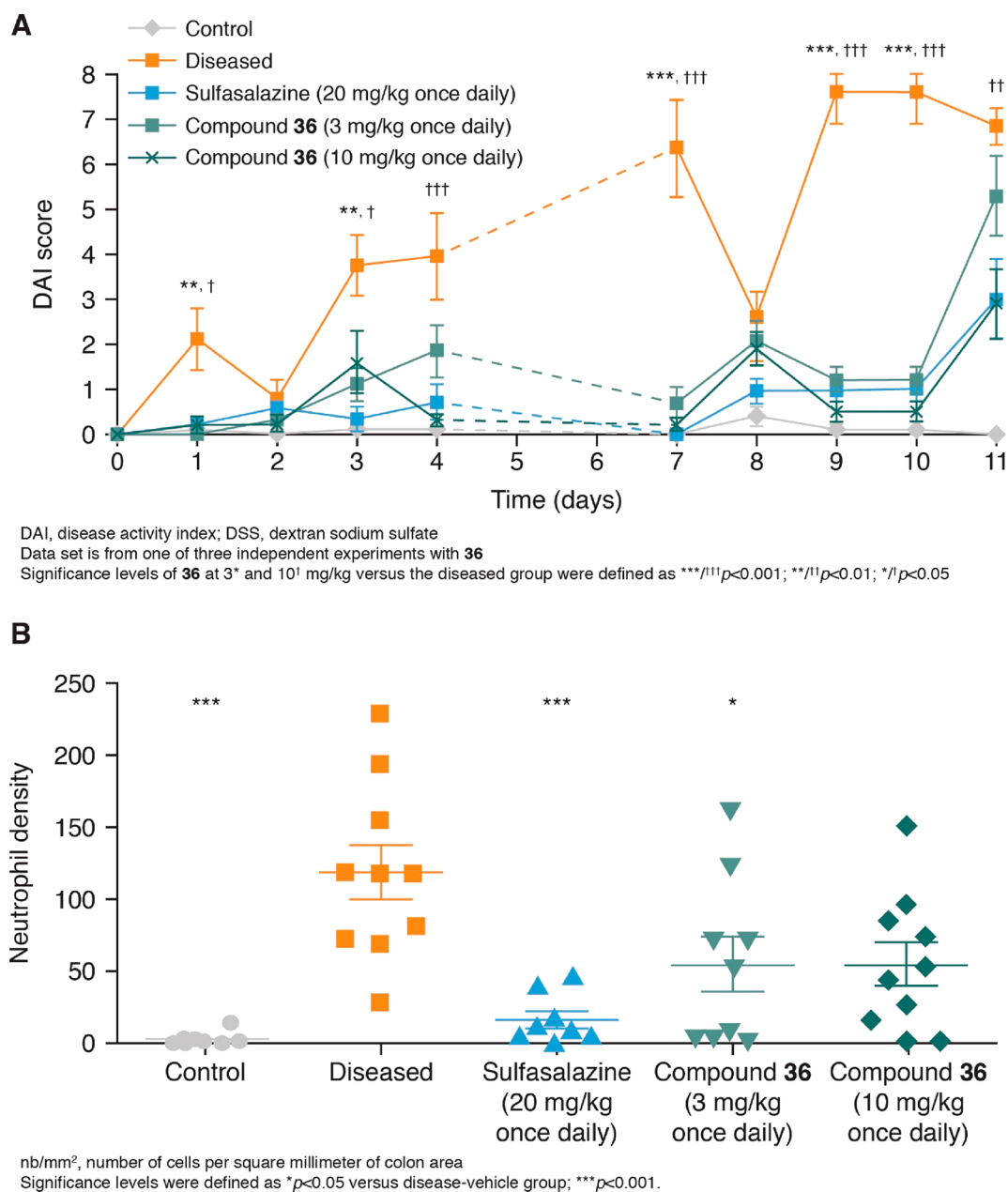
**Chemistry. Methods.** All reagents were of commercial grade and were used as received without further purification unless otherwise stated. Commercially available anhydrous solvents were used for reactions conducted under inert atmosphere. Reagent grade solvents were used in all other cases unless otherwise specified. Column chromatography was performed on silica gel 60 (35–70 μm). Thin layer chromatography was carried out using precoated silica gel F-254 plates (thickness 0.25 mm). Microwave heating was performed with a Biotage Initiator apparatus (Biotage, Uppsala, Sweden). Celpure P65 (Merck KGaA, Darmstadt, Germany) is a filtration aid and commercial product (CAS number 61790-53-2). <sup>1</sup>H NMR spectra were recorded on a Bruker DPX 400 NMR spectrometer (400 MHz) (Bruker, Billerica, MA, USA) or a Bruker Avance 300 NMR spectrometer (300 MHz) (Bruker, Billerica, MA, USA). Chemical shifts (δ) for <sup>1</sup>H NMR spectra are reported in parts per million (ppm) relative to tetramethylsilane (δ 0.00) or the appropriate residual solvent peak, i.e., CHCl<sub>3</sub> (δ 7.27), as internal reference. Multiplicities are given as singlet (s), doublet (d), triplet (t), quartet (q), quintuplet (quin), multiplet (m), and broad (br). Waters Acquity UPLC (Waters, Elstree, U.K.) with Waters Acquity PDA detector (Waters, Elstree, U.K.) and SQD mass spectrometer (Waters, Elstree, U.K.) were used to generate UV and MS chromatograms as well as MS spectra. Columns used were the following: UPLC BEH C18 1.7 μm, 2.1 mm



**Figure 4.** (A) Effect of increasing concentrations of 36 on effects of orthosteric and allosteric GPR84 agonists (GTPyS assay with agonists used at EC<sub>80</sub>). (B) Structure of tritiated ligand 38. (C) Ability of various concentrations of C10, PSB-16671, and 36 to compete for binding with [<sup>3</sup>H]38 to GPR84 (competition binding + 0.2 nM [<sup>3</sup>H]38). (D) Schild analysis showing inhibition of PSB-16671 activity with 36 at concentrations of 10 nM, 30 nM, 100 nM, and 300 nM.

× 5 mm, VanGuard Precolumn (Waters, Elstree, U.K.) with Acquity UPLC BEH C18 1.7 μm, 2.1 mm × 30 mm column or Acquity UPLC BEH C18 1.7 μm, 2.1 mm × 50 mm column. LC-MS analyses were

conducted using the following two methods. Method 1: solvent A, H<sub>2</sub>O–0.05% NH<sub>4</sub>OH; solvent B, MeCN–0.05% NH<sub>4</sub>OH; flow rate, 0.8 mL/min; start 5% B, final 95% B in 1.55 min, linear gradient.



**Figure 5.** Diseased mice (DSS-induced chronic colitis model) were administered with 4% DSS in drinking water for 4 days, followed by 3 days of regular drinking water and a new cycle of DSS. In addition they were orally administered **36** at 3\* and 10<sup>1</sup> mg/kg qd, sulfasalazine 20 mg/kg qd (positive control) or vehicle, for 11 consecutive days. Control mice were administered water alone as a negative control. (A) Disease activity index score. Data are the mean  $\pm$  SEM. No scores were measured on days 5 and 6. (B) Neutrophil density (number of cells per square millimeter of colon area, as determined by immunohistochemistry assay with anti-Ly6G/Ly6C antibodies).

Method 2: solvent A, H<sub>2</sub>O–0.1% HCO<sub>2</sub>H; solvent B, MeCN–0.1% HCO<sub>2</sub>H; flow rate, 0.8 mL/min; start 5% B, final 95% B in 1.55 min, linear gradient. All final compounds reported were analyzed using one of these analytical methods, and purity is greater than 95% or otherwise indicated in the Supporting Information. Autopurification system from Waters was used for LC–MS purification. LC–MS columns used: Waters XBridge Prep OBD C18 5  $\mu$ m, 30 mm  $\times$  100 mm (preparative column) and Waters XBridge BEH C18 5  $\mu$ m, 4.6 mm  $\times$  100 mm (analytical column) (Waters, Elstree, U.K.). All the methods used MeCN/H<sub>2</sub>O gradients. MeCN and H<sub>2</sub>O contained either 0.1% formic acid or 0.1% diethylamine.

**2-(3-Methoxyphenyl)ethylurea.** A solution of 3-methoxyphenethylamine (100 g, 661.3 mmol), urea (157.3 g, 2619.0 mmol), glacial AcOH (36 mL), and concentrated HCl (12 mL) in H<sub>2</sub>O (800 mL) was heated under reflux for 5 days. The reaction mixture was

cooled to room temperature (RT), and the precipitate obtained was filtered off, washed with water, and dried under vacuum to give 2-(3-methoxyphenyl)ethylurea as a white solid (92 g, 72% yield). <sup>1</sup>H NMR (400 MHz, methanol-*d*<sub>4</sub>)  $\delta$  7.18 (t, *J* = 8.1 Hz, 1H), 6.83–6.71 (m, 3H), 3.77 (s, 3H), 3.37–3.31 (m, 2H), 2.74 (t, *J* = 7.2 Hz, 2H).

**2-(3-Hydroxyphenyl)ethylurea.** A solution of 2-(3-methoxyphenyl)ethylurea (92 g, 473.6 mmol) in concentrated HBr (600 mL) was heated under reflux overnight. The reaction was cooled to RT and basified by addition of NaHCO<sub>3</sub> and extracted with EtOAc. The organic layer was dried over MgSO<sub>4</sub>, filtered, and concentrated under reduced pressure to give crude 2-(3-hydroxyphenyl)ethylurea as a light brown solid (67 g) which was used in the next step without further purification. <sup>1</sup>H NMR (400 MHz, DMSO-*d*<sub>6</sub>)  $\delta$  9.25 (s, 1H), 7.07 (td, *J* = 7.2, 1.8 Hz, 1H), 6.65–

**Table 9. Pharmacokinetic Parameters of 36 at Steady State in Female BALB/c Mice after Multiple Oral Doses of 3 or 10 mg kg<sup>-1</sup> day<sup>-1</sup> <sup>a</sup>**

		3 mg kg <sup>-1</sup> day <sup>-1</sup> (n = 2 or 3)	10 mg kg <sup>-1</sup> day <sup>-1</sup> (n = 2 or 3)
C <sub>max</sub>	(ng/mL)	1837	8140
C <sub>max</sub> /dose		612	814
T <sub>max</sub>	(h)	1	1
AUC <sub>(0-24h)</sub>	(ng·h/mL)	5556	50387
AUC <sub>(0-24h)</sub> /dose		1852	5039
t <sub>1/2</sub>	(h)	2.9	2.3

<sup>a</sup>Abbreviations: AUC, area under curve; C<sub>max</sub>, maximum plasma concentration; T<sub>max</sub>, time to C<sub>max</sub>; t<sub>1/2</sub>, half-life.

6.55 (m, 3H), 5.89 (t, J = 5.8 Hz, 1H), 3.16 (dt, J = 7.7, 6.3 Hz, 2H), 2.57 (t, J = 7.3 Hz, 2H). LCMS: m/z 181 [M + H]<sup>+</sup>.

**2-(3-Allyloxyphenyl)ethylurea.** To a solution of crude 2-(3-hydroxyphenyl)ethylurea (67 g, 371.0 mmol) and K<sub>2</sub>CO<sub>3</sub> (154 g, 1115.0 mmol) in DMF (400 mL) was added allyl bromide (75 mL, 743.6 mmol), and the reaction was stirred for 2.5 days. DMF was concentrated under reduced pressure and then the residue was dissolved in EtOAc, washed with a saturated aqueous solution of Na<sub>2</sub>CO<sub>3</sub> followed by brine, then dried over MgSO<sub>4</sub>. Concentration under reduced pressure gave crude 2-(3-allyloxyphenyl)ethylurea as a colorless solid (79 g) which was used in the next step without further purification. <sup>1</sup>H NMR (400 MHz, methanol-d<sub>4</sub>) δ 7.97 (s, 1H), 7.22–7.13 (m, 1H), 6.84–6.71 (m, 3H), 6.13–5.97 (m, 1H), 5.39 (dq, J = 17.3, 1.7 Hz, 1H), 5.23 (dq, J = 10.6, 1.6 Hz, 1H), 4.52 (ddt, J = 5.1, 3.5, 1.6 Hz, 2H), 3.34 (d, J = 7.0 Hz, 2H), 2.98 (d, J = 0.6 Hz, 2H), 2.74 (t, J = 7.3 Hz, 2H). LCMS: m/z 221 [M + H]<sup>+</sup>.

**1-[2-(3-Allyloxyphenyl)ethyl]hexahydropyrimidine-2,4,6-trione.** To a stirred solution of sodium (16 g, 718.0 mmol) in EtOH (1.0 L), diethyl malonate (109.1 mL, 718.0 mmol) was added, and the reaction mixture was heated under reflux for 1 h. Crude 2-(3-allyloxyphenyl)ethylurea (72 g, 359.0 mmol) in EtOH (200 mL) was added, and the reaction mixture was heated under reflux for 12 h. The reaction was cooled to RT, 1 M aq HCl was added, and the precipitate obtained was filtered off, washed with water, and dried under vacuum to give 1-[2-(3-allyloxyphenyl)ethyl]hexahydropyrimidine-2,4,6-trione as a yellow solid (82 g, 79% yield). <sup>1</sup>H NMR (400 MHz, CDCl<sub>3</sub>) δ 8.36 (s, 1H), 7.25–7.16 (m, 1H), 6.87–6.72 (m, 3H), 6.05 (ddt, J = 17.3, 10.5, 5.3 Hz, 1H), 5.41 (dq, J = 17.3, 1.6 Hz, 1H), 5.28 (dq, J = 10.5, 1.4 Hz, 1H), 4.53 (dt, J = 5.3, 1.5 Hz, 2H), 4.15–4.04 (m, 2H), 3.61 (s, 2H), 2.92–2.82 (m, 2H). LCMS: m/z 289 [M + H]<sup>+</sup>.

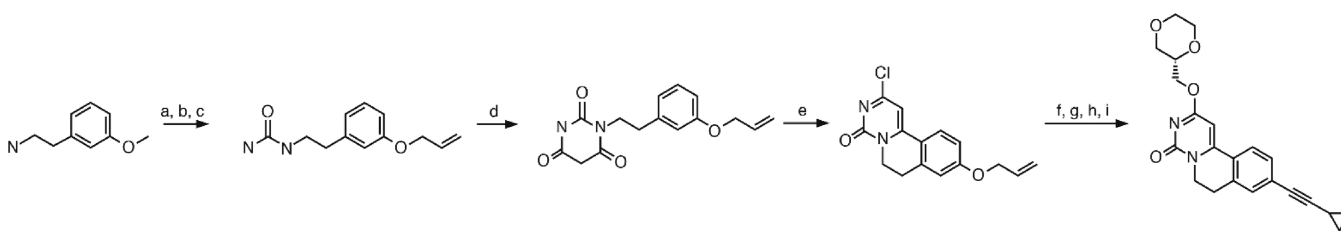
**9-Allyloxy-2-chloro-6,7-dihydropyrimido[6,1-a]isoquinolin-4-one.** A solution of 1-[2-(3-allyloxyphenyl)ethyl]hexahydropyrimidine-2,4,6-trione (50 g, 173.4 mmol) in POCl<sub>3</sub> (100 mL) was stirred at 50 °C for 3 days. POCl<sub>3</sub> was concentrated under pressure, and the residue was dissolved in dichloromethane (DCM) and quenched with a saturated aqueous solution of NaHCO<sub>3</sub>. The organic layer was washed with water, dried over MgSO<sub>4</sub>, filtered,

and concentrated under reduced pressure to give crude 9-allyloxy-2-chloro-6,7-dihydropyrimido[6,1-a]isoquinolin-4-one as a yellow solid (46 g, 92% yield). <sup>1</sup>H NMR (400 MHz, CDCl<sub>3</sub>) δ 7.67 (d, J = 8.8 Hz, 1H), 6.94 (dd, J = 8.8, 2.6 Hz, 1H), 6.85–6.80 (m, 1H), 6.67 (s, 1H), 6.04 (ddt, J = 17.2, 10.5, 5.2 Hz, 1H), 5.43 (dq, J = 17.3, 1.6 Hz, 1H), 5.34 (dq, J = 10.5, 1.4 Hz, 1H), 4.62 (dt, J = 5.3, 1.5 Hz, 2H), 4.26–4.19 (m, 2H), 3.01 (t, J = 6.7 Hz, 2H). LCMS: m/z 289 [M + H]<sup>+</sup>.

**9-Allyloxy-2-[[[(2S)-1,4-dioxan-2-yl]methoxy]-6,7-dihydropyrimido[6,1-a]isoquinolin-4-one.** To a solution of (R)-2-hydroxymethyl[1,4]dioxane (1.82 g, 15.4 mmol) in anhydrous DCM (100 mL) under N<sub>2</sub> at 0 °C, NaH (618 mg, 15.4 mmol, 60% in mineral oil) was added and stirred for 15 min. 9-Allyloxy-2-chloro-6,7-dihydropyrimido[6,1-a]isoquinolin-4-one (3.43 g, 11.9 mmol) was added, and the reaction mixture was stirred and warmed up to RT overnight. Saturated NH<sub>4</sub>Cl was added, and the organic layer was washed with water, dried over MgSO<sub>4</sub>, and concentrated under reduced pressure. The crude product was purified by flash chromatography on silica gel eluting with 5% MeOH in DCM to afford 9-allyloxy-2-[[[(2S)-1,4-dioxan-2-yl]methoxy]-6,7-dihydropyrimido[6,1-a]isoquinolin-4-one as a yellow solid (2.90 g, 66% yield). <sup>1</sup>H NMR (400 MHz, DMSO-d<sub>6</sub>) δ 7.95 (d, J = 8.7 Hz, 1H), 7.02–6.93 (m, 2H), 6.54 (s, 1H), 6.06 (ddt, J = 17.3, 10.5, 5.2 Hz, 1H), 5.42 (dq, J = 17.3, 1.7 Hz, 1H), 5.29 (dq, J = 10.6, 1.5 Hz, 1H), 4.67 (dt, J = 5.3, 1.5 Hz, 2H), 4.30–4.20 (m, 2H), 4.06–3.98 (m, 2H), 3.85 (dddd, J = 10.0, 5.9, 4.4, 2.6 Hz, 1H), 3.78 (td, J = 10.7, 10.1, 2.8 Hz, 2H), 3.70–3.56 (m, 2H), 3.49 (td, J = 10.8, 2.7 Hz, 1H), 3.38 (dd, J = 11.4, 9.9 Hz, 1H), 2.97 (t, J = 6.5 Hz, 2H). LCMS: m/z 371 [M + H]<sup>+</sup>.

**2-[[[(2S)-1,4-Dioxan-2-yl]methoxy]-9-hydroxy-6,7-dihydropyrimido[6,1-a]isoquinolin-4-one.** To a suspension of 9-allyloxy-2-[[[(2S)-1,4-dioxan-2-yl]methoxy]-6,7-dihydropyrimido[6,1-a]isoquinolin-4-one (31.2 g, 84.2 mmol) in a mixture of DCM/MeOH (300 mL/300 mL), K<sub>2</sub>CO<sub>3</sub> (23.27 g, 168.4 mmol) and Pd(PPh<sub>3</sub>)<sub>4</sub> (4.86 g, 4.21 mmol) were added, and the reaction mixture was degassed before stirring at RT overnight. After completion, the reaction was quenched with H<sub>2</sub>O, the aqueous layer was separated, and the pH was adjusted to pH 1 with 2 M aq HCl, and the precipitate formed was filtered off, washed with water, and dried to afford 2-[[[(2S)-1,4-dioxan-2-yl]methoxy]-9-hydroxy-6,7-dihydropyrimido[6,1-a]isoquinolin-4-one as a yellow solid (18.62 g, 67% yield). <sup>1</sup>H NMR (400 MHz, DMSO-d<sub>6</sub>) δ 10.32 (s, 1H), 7.83 (d, J = 8.6 Hz, 1H), 6.77 (dd, J = 8.6, 2.5 Hz, 1H), 6.74 (d, J = 2.4 Hz, 1H), 6.44 (s, 1H), 4.28–4.18 (m, 2H), 4.03–3.94 (m, 2H), 3.89–3.72 (m, 3H), 3.69–3.56 (m, 2H), 3.49 (td, J = 10.8, 2.7 Hz, 1H), 3.37 (dd, J = 11.4, 9.9 Hz, 1H), 2.91 (t, J = 6.5 Hz, 2H). LCMS: m/z 331 [M + H]<sup>+</sup>.

**[2-[[[(2S)-1,4-Dioxan-2-yl]methoxy]-4-oxo-6,7-dihydropyrimido[6,1-a]isoquinolin-9-yl] Trifluoromethanesulfonate.** A solution of 2-[[[(2S)-1,4-dioxan-2-yl]methoxy]-9-hydroxy-6,7-dihydropyrimido[6,1-a]isoquinolin-4-one (23.25 g, 70.5 mmol), N-phenyl-bis(trifluoromethanesulfonamide) (27.69 g, 77.5 mmol), and Et<sub>3</sub>N (17.5 mL, 126.8 mmol) in DCM (800 mL) under N<sub>2</sub> was stirred at RT for 5 h. The reaction mixture was concentrated, and the crude product was purified by recrystallization from iPrOH to afford

**Scheme 1. Synthesis of (S)-GLPG1205 (36) <sup>a</sup>**

<sup>a</sup>Reagents and conditions: (a) urea, AcOH, conc HCl, water, reflux; (b) conc HBr, reflux; (c) AllylBr, K<sub>2</sub>CO<sub>3</sub>, DMF; (d) Na, EtOH, diethyl malonate, reflux; (e) POCl<sub>3</sub>, 50 °C; (f) [(2R)-1,4-dioxan-2-yl]methanol, tBuOK, DCM; (g) Pd(PPh<sub>3</sub>)<sub>4</sub>, K<sub>2</sub>CO<sub>3</sub>, MeOH/THF; (h) PhN(SO<sub>2</sub>CF<sub>3</sub>)<sub>2</sub>, Et<sub>3</sub>N, DCM; (i) ethynylcyclopropane, Pd(PPh<sub>3</sub>)<sub>4</sub>, CuI, Et<sub>3</sub>N, DMF.

[2-[[[(2S)-1,4-dioxan-2-yl]methoxy]-4-oxo-6,7-dihydropyrimido[6,1-*a*]isoquinolin-9-yl] trifluoromethanesulfonate as a white solid (24.5 g, 75% yield). <sup>1</sup>H NMR (400 MHz, CDCl<sub>3</sub>) δ 7.79 (d, *J* = 8.7 Hz, 1H), 7.31 (dd, *J* = 8.7, 2.6 Hz, 1H), 7.27–7.23 (m, 1H), 6.37 (s, 1H), 4.50–4.35 (m, 2H), 4.24 (dd, *J* = 7.1, 5.8 Hz, 2H), 4.02–3.93 (m, 1H), 3.90–3.69 (m, 4H), 3.65 (ddd, *J* = 11.7, 10.6, 3.0 Hz, 1H), 3.48 (dd, *J* = 11.5, 10.1 Hz, 1H), 3.07 (t, *J* = 6.5 Hz, 2H). LCMS: *m/z* 463 [M + H]<sup>+</sup>.

**9-(2-Cyclopropylethynyl)-2-[[[(2S)-1,4-dioxan-2-yl]methoxy]-6,7-dihydropyrimido[6,1-*a*]isoquinolin-4-one (36).** To a solution of [2-[[[(2S)-1,4-dioxan-2-yl]methoxy]-4-oxo-6,7-dihydropyrimido[6,1-*a*]isoquinolin-9-yl] trifluoromethanesulfonate (42 g, 90.8 mmol) in anhydrous DMF (840 mL), cyclopropylacetylene (15.38 mL, 181.6 mmol) was added followed by Et<sub>3</sub>N (31.5 mL, 227.0 mmol), and the mixture was degassed. Pd(PPh<sub>3</sub>)<sub>2</sub>Cl<sub>2</sub> (3.19 g, 4.5 mmol) was added with CuI (3.46 g, 18.2 mmol), and the reaction mixture was heated at 50 °C overnight. The reaction mixture was concentrated and the crude was purified by flash chromatography on silica gel eluting with 1–3% MeOH in DCM to afford 9-(2-cyclopropylethynyl)-2-[[[(2S)-1,4-dioxan-2-yl]methoxy]-6,7-dihydropyrimido[6,1-*a*]isoquinolin-4-one as a light brown solid (30.2 g, 88% yield). <sup>1</sup>H NMR (400 MHz, CDCl<sub>3</sub>) δ 7.57 (d, *J* = 8.2 Hz, 1H), 7.32 (dd, *J* = 8.2, 1.6 Hz, 1H), 6.31 (s, 1H), 4.45–4.32 (m, 2H), 4.16 (dd, *J* = 7.0, 5.9 Hz, 2H), 4.00–3.90 (m, 1H), 3.87–3.57 (m, 5H), 3.45 (dd, *J* = 11.5, 10.1 Hz, 1H), 2.93 (t, *J* = 6.5 Hz, 2H), 1.45 (tt, *J* = 8.2, 5.0 Hz, 1H), 0.94–0.85 (m, 2H), 0.85–0.75 (m, 2H). LCMS: 0.70 min, *m/z* 379.5 [M + H]<sup>+</sup>. Chromatographic conditions: Waters Alliance HPLC, column Daicel Chiralpak (Chiral Technologies, West Chester, PA, USA) IG 4.6 mm i.d. × 250 mm, 5 μm particle size, wavelength 330 nm, flow rate 0.8 mL/min, column temperature 25 °C, injection volume 10 μL, run time 65 min, isocratic elution (85/15) *tert*-butyl methyl ether/ethanol, retention time 32.87 min.

**Biology. HTS.** The cAMP assay measures the level of Gi protein activation following agonist occupancy of GPR84, in the presence of forskolin to stimulate production of cAMP, and adenylate cyclase and 3-isobutyl-1-methylxanthine (IBMX) to block phosphodiesterase activity. HEK293T samples stably transfected with recombinant human GPR84 (Multiscreen; Multispan, Hayward, CA, USA) were seeded at a density of 2500 cells/well in a 384-well plate in suspension on the day of the assay in assay buffer (1× Hanks' balanced salt solution [HBSS]), 20 mM (4-(2-hydroxyethyl)-1-piperazineethanesulfonic acid (HEPES), 0.5 mM IBMX). GPR84 was stimulated with capric acid as the natural ligand at EC<sub>85</sub> (30.5 μM), and tested compounds were added simultaneously for 30 min before the addition of 1.5 μM forskolin for 30 min. Cells were lysed and analyzed for cAMP level using a competitive immunoassay in homogeneous time-resolved fluorescence (HTRF) format (Cisbio, Bedford, MA, USA). Fluorescence signals were read on a PerkinElmer ViewLux1430 microplate imager (PerkinElmer, Boston, MA, USA).

**Recombinant Human GPR84 GTPγS Binding Assay.** The assay was performed in a 96-well plate where the following reagents were added. First, 50 μL of hit compound from HTS was added into the assay plate, followed by addition of 20 μL of DIM at EC<sub>80</sub> concentration (concentration which gives 80% of the activity of GPR84) and was incubated with 30 μL of mixture consisting of membranes derived from stable cell line overexpressing recombinant human GPR84, [<sup>35</sup>S]GTPγS, and scintillation proximity assay (SPA) beads (PerkinElmer, Boston, MA, USA; RPNQ0001). All components were diluted in assay buffer containing 20 mM HEPES, pH 7.4; 5 mM MgCl<sub>2</sub>; 250 mM NaCl; 0.05% bovine serum albumin (BSA); 75 μg/mL saponin. Reactions were incubated at room temperature for 90 min followed by centrifugation. Plates were read on a Topcount reader (Molecular Devices, Sunnyvale, CA, USA) immediately after centrifugation.

**IP1 Assay.** The IP1 assay using transiently transfected cells allowed the development of similar assays with overexpression of either mouse or human GPR84. IP1 activity was measured in HEK293T cells transiently transfected with a variant of Gq protein (GNAO1 transcription variant 1) and GPR84 using the Cisbio IP-

One assay, which detected the accumulation of IP1, a stable downstream metabolite of IP3 induced by activation of a phospholipase C (PLC) cascade.

HEK293T cells were transiently transfected in suspension with a variant of Gq protein and recombinant mouse or human GPR84 using Jet-PEI (Polyplus-transfection, Sebastian Brant, France) and seeded at a density of 25 000 cells/well in a 384-well plate. After overnight incubation, the transfection mix was removed and replaced by cell culture medium for 24 h. The cells were then treated with test compounds for 30 min before addition of capric acid at EC<sub>80</sub> for 1 h for the human assay. As transfection of mouse GPR84 resulted in IP1 activity in the absence of capric acid stimulation, compounds were tested in inverse agonist mode without addition of capric acid. IP1 was measured using competitive immunoassay in HTRF format (Cisbio, Bedford, CA, USA) according to manufacturer's instructions. Fluorescence signal was read on PerkinElmer EnVision (PerkinElmer, Boston, MA, USA).

**PDE4A Inhibition.** The IC<sub>50</sub> value for human PDE4A was determined in a HTRF based cAMP assay. PDE4A present in a HEK293 cell lysate containing overexpressed PDE4A hydrolyzes cAMP into 5'AMP. The amount of cAMP present is measured in a competitive immunoassay, which is based on competition between native cAMP and d2-labeled cAMP for binding to an anti-cAMP monoclonal antibody labeled with cryptate. The specific signal (i.e., energy transfer) is inversely proportional to the concentration of cAMP.

**Human Neutrophil Migration.** Freshly isolated human neutrophils were diluted in a suspension of 8.9 × 10<sup>6</sup> cells per mL. 20 μL of compound solution in chemotaxis buffer was added to the 180 μL cell suspension. The mixture was incubated at 37 °C for 30 min with intermediate resuspension of the cells after 15 min. Following this, 70 μL of cell suspension was transferred to the upper compartment of a Corning HTS Transwell 96 permeable support system with 5.0 μm pore size polycarbonate membrane (Corning, Corning, NY, USA; catalog no. 3387). The receiver well of the Transwell system was then filled with 200 μL of chemotaxis buffer containing compound and chemotactic agent (embelin). After incubation at 37 °C in 5% CO<sub>2</sub> for 1 h, the upper plate of the Transwell system was removed and the cell suspension in the receiver plate is transferred to a 96-well V-bottom plate. 50 μL of DPBS was added to the receiver plate to prevent remaining cells from drying out. The V-bottom plate was centrifuged for 6 min at 1500 rpm. The supernatant was removed, and the cells were resuspended in 50 μL DPBS. The cells were then transferred back to the receiver plate of the Transwell system. After this, 100 μL of ATPlite solution (PerkinElmer, Boston, MA, USA; catalog no. 436110) was added to the cells. The plate was incubated for 10 min in the dark while shaking. 170 μL of cell lysate was then transferred to a white 96-well plate, and luminescence was measured. The detected luminescent signal was considered as linearly related to the number of cells having migrated from the upper well to the receiver well.

**Rat Neutrophil Migration.** Freshly isolated rat neutrophils were diluted in a suspension of 8.9 × 10<sup>6</sup> cells per mL. 10 μL of compound solution in chemotaxis buffer was added to the 90 μL cell suspension. The mixture was incubated at 37 °C for 30 min with intermediate resuspension of the cells after 15 min. Following this, 75 μL of cell suspension was transferred to the upper compartment of a Corning HTS Transwell 96 permeable support system with 5.0 μm pore size polycarbonate membrane (Corning, Corning, NY, USA; catalog no. 3387). The receiver well of the Transwell system was then filled with 200 μL of chemotaxis buffer containing compound and chemotactic agent (embelin). After incubation at 37 °C in 5% CO<sub>2</sub> for 1 h, the upper plate of the Transwell system was removed and 70 μL of CellTiter-Glo substrate (Promega, Madison, WI, USA; catalog no. G755B) was added to a 96-well V-bottom plate. The plate was incubated for 10 min in the dark while shaking. 180 μL of cell lysate was then transferred to a white 96-well plate, and luminescence was measured. The detected luminescent signal was considered as linearly related to the number of cells having migrated from the upper well to the receiver well.

**Liver Microsomal Stability (LMS) Assay.** The microsomal stability assay was performed by incubation of test compound at 1  $\mu\text{M}$ , 0.2% DMSO in phosphate buffer with microsomes (0.5 mg/mL) from mouse, rat, dog, or human (Xeno-Tech, Kansas City, KS, USA), and cofactors with final concentrations of 0.6 U/mL glucose-6-phosphate dehydrogenase, 3.3 mM  $\text{MgCl}_2$ , 3.3 mM glucose-6-phosphate, and 1.3 mM nicotinamide adenine dinucleotide phosphate (NADP)<sup>+</sup>. Before addition of the microsomes (time zero) and after 30 min of incubation at 37 °C with shaking, the reaction was stopped and proteins were precipitated with an excess of acetonitrile containing an internal standard. The samples were mixed, centrifuged, and filtered, and the supernatant was analyzed by liquid chromatography–mass spectrometry/mass spectrometry (LC–MS/MS). The instrument responses (peak areas/IS peak area) were referenced to the zero-time point samples (considered as 100%) in order to determine the percentage of compound remaining. Verapamil (1  $\mu\text{M}$ ) and warfarin (1  $\mu\text{M}$ ) were used as reference compounds, as unstable and stable compounds, respectively.

*In vitro* scaled intrinsic clearance ( $\text{CL}_{\text{int}}$  scaled) was calculated from the half-life using the following equations:

(1) Intrinsic clearance equation:

$$\text{CL}_{\text{int}} [\mu\text{L mg}^{-1} \text{min}^{-1}] = \frac{\ln 2}{t_{1/2} [\text{min}]} \times \frac{\text{incubation volume } [\mu\text{L}]}{\text{mg of protein}}$$

(2) Scaled intrinsic clearance equation:

$$\text{scaled CL}_{\text{int}} [\text{L h}^{-1} \text{kg}^{-1}] = \text{CL}_{\text{int-in vitro}} [\mu\text{L mg}^{-1} \text{min}^{-1}] \times \frac{\text{mg of microsomal protein}}{\text{g of liver}} \times \frac{\text{liver weight (g)}}{\text{body weight (kg)}} \times \frac{60}{1000000}$$

**Hepatocyte Stability Assay.** The hepatocyte stability assay was performed by incubation of test compound at 1  $\mu\text{M}$ , 0.03% DMSO in modified Krebs–Henseleit buffer with suspension of pooled cryopreserved hepatocytes (BioIVT, Hicksville, NY, USA) from mouse, rat, dog, or human (BioIVT, Hicksville, NY, USA) at 0.5 million viable hepatocytes/mL.

Before adding the hepatocytes (time zero) and after 10, 20, 45, 90, 120, and 180 min of incubation ( $n = 2$ ) at 37 °C while gently shaking, the reaction was stopped and proteins were precipitated with an excess of acetonitrile containing an internal standard. The samples were mixed, centrifuged, and filtered, and the supernatant was analyzed by liquid chromatography–mass spectrometry/mass spectrometry (LC–MS/MS). The instrument responses (peak areas/IS peak area) were referenced to the zero-time point samples (considered as 100%) in order to determine the percentage of compound remaining. Testosterone (1  $\mu\text{M}$ ) and 7-hydroxycoumarin (1  $\mu\text{M}$ ) were used as phase I and phase II reaction controls, while caffeine was used as a negative control.

*In vitro* intrinsic clearance ( $\text{CL}_{\text{int}}$ ) was calculated from half-life using the following equations:

$$\text{CL}_{\text{int}} [(\mu\text{L}/\text{min})/10^6 \text{ cells}] = \frac{\ln 2}{t_{1/2} [\text{min}]} \times \frac{\text{incubation volume } [\mu\text{L}]}{\text{no. cells per incubation}}$$

$$\text{scaled CL}_{\text{int}} [\text{L h}^{-1} \text{kg}^{-1}] = \text{CL}_{\text{int-in vitro}} [(\mu\text{L}/\text{min})/10^6 \text{ cells}] \times \frac{10^6 \text{ cells}}{\text{g of liver}} \times \frac{\text{liver weight (g)}}{\text{body weight (kg)}} \times \frac{60}{1000000}$$

**Plasma Protein Binding Assay.** Plasma protein binding was determined by equilibrium dialysis using the Pierce Red device plate with inserts (Thermo Fisher Scientific, Waltham, MA, USA). Test compound at 5  $\mu\text{M}$  (0.5% DMSO) spiked in freshly thawed human, rat, mouse, or dog plasma (Bioreclamation INC, Westbury, NY, USA) was dialyzed against phosphate-buffered saline (PBS, pH 7.4) at 37 °C under shaking for 4 h. Proteins were precipitated with an excess of methanol, and samples were mixed and centrifuged, and the supernatant was analyzed by liquid chromatography–mass spectrometry/mass spectrometry (LC–MS/MS).

etry/mass spectrometry (LC–MS/MS). Addition of compound peak areas in the buffer chamber and the plasma chamber was considered to be 100% compound. The percentage bound to plasma proteins was derived from these results with the formula

$$\% \text{ bound} = 100 \times \frac{\text{peak area of plasma} - \text{peak area of buffer}}{\text{peak area of plasma}}$$

Acebutolol and nicardipine are included in the assay design as low and high binding controls.

**Intestinal Permeability on Caco-2 Cells.** Caco-2 cells were obtained from European Collection of Cell Cultures (ECACC) and used after a 21-day cell culture in 24-well Transwell plates.

GLPG1205 and the references (vinblastine and propranolol) were prepared in protein-free Hanks' balanced salt solution containing 25 mM HEPES (pH 7.4) at a concentration of 10  $\mu\text{M}$  and added to either the apical or basolateral chambers of a Transwell plate assembly.

Before the experiment, the integrity of the monolayer was checked by measuring the transepithelial resistance. Lucifer yellow (LY) was added to the donor buffer in all wells to assess integrity of the cell layers by monitoring LY permeation. As LY cannot freely permeate lipophilic barriers, a high degree of LY transport indicates poor integrity of the cell layer.

After a 1 h incubation at 37 °C, aliquots were taken from both apical (A) and basolateral (B) chambers and added to acetonitrile containing analytical internal standard (carbamazepine) in a 96-well plate. Concentrations of compound in the samples were measured by LC–MS/MS.

Apparent permeability ( $P_{\text{app}}$ ) values were calculated from the relationship

$$P_{\text{app}} = \frac{[\text{compound}]_{\text{acceptor final}} V_{\text{acceptor}} / ([\text{compound}]_{\text{donor initial}} V_{\text{donor}})}{T_{\text{inc}} V_{\text{donor}} / (\text{surface area} \times 60 \times 10^{-6} \text{ cm/s})}$$

where  $V_{\text{donor}}$  is the volume of the apical chamber at 125  $\mu\text{L}$ ,  $V_{\text{acceptor}}$  is the volume of the basolateral chamber at 600  $\mu\text{L}$ ,  $T_{\text{inc}}$  is the incubation time of 3600 s, and the surface area for the 24-well Transwell is 0.33  $\text{cm}^2$ . The efflux ratios, as an indication of active efflux from the apical cell surface, were calculated using the ratio of  $P_{\text{app}}(\text{B} \rightarrow \text{A})/P_{\text{app}}(\text{A} \rightarrow \text{B})$ .

**CYP Direct Inhibition Assay.** A 5 mM stock solution of compound was prepared in methanol. This stock was serially diluted 1:3 in methanol and then added in duplicates to a mixture containing 50 mM potassium phosphate buffer, pH 7.4, and human liver microsomes (BD Gentest, BD, Wokingham, U.K.). A total of seven different concentrations (0.14–100  $\mu\text{M}$  in final reaction mixture; 2% methanol) of compound were prepared in duplicates.

After prewarming for 5 min at 37 °C, the 20 min preincubation was started by adding a probe substrate to the first concentration range (first replica) and a cofactor mix (7.65 mg/mL glucose-6-phosphate, 1.7 mg/mL NADP, 6 U/mL of glucose-6-phosphate dehydrogenase) to the second replica. Final concentrations of cofactor mix components were as follows: 1.56 mg/mL glucose-6-phosphate, 0.34 mg/mL NADP, 1.2 U/mL of glucose-6-phosphate dehydrogenase.

After preincubation, the reaction was finally started by adding the cofactor mix to the first replica and adding the probe substrate to second replica (opposite from preincubation).

After incubation at 37 °C, the reaction (aliquot of 50  $\mu\text{L}$ ) was terminated with 150  $\mu\text{L}$  of acetonitrile/methanol (2:1) solution with internal standard (diclofenac). Samples were centrifuged and the supernatant fractions analyzed by LC–MS/MS.

The instrument responses (ratio of compound and internal standard peak areas) were referenced to those for solvent controls (assumed as 100%) in order to determine the percentage reduction in probe metabolism.

Percent of control activity versus concentration plots were generated and fitted using GraphPad Prism software to determine



IC<sub>50</sub> for both substrate- and cofactor preincubations, as well as the IC<sub>50</sub> fold shift.

**hERG Manual Patch Clamp Assay.** Whole-cell patch-clamp recordings were performed using an EPC10 amplifier controlled by Pulse version 8.77 software (HEKA, Ludwigshafen, Germany). The external bathing solution contained 135 mM NaCl, 5 mM KCl, 1.8 mM CaCl<sub>2</sub>, 5 mM glucose, 10 mM HEPES, pH 7.4. The internal patch pipet solution contained 100 mM K gluconate, 20 mM KCl, 1 mM CaCl<sub>2</sub>, 1 mM MgCl<sub>2</sub>, 5 mM Na<sub>2</sub>ATP, 2 mM glutathione, 11 mM ethylene glycol-bis( $\beta$ -aminoethyl ether)-*N,N,N',N'*-tetraacetic acid (EGTA), 10 mM HEPES, pH 7.2. Compound was perfused using an automate scientific pressurized superfusion system coupled to a Biologic micromanifold.

All recordings were performed on HEK293 cells stably expressing hERG channels. Cells were cultured on 12 mm round coverslips (German glass; Bellco, Vineland, NJ, USA) anchored in the recording chamber using two platinum rods (Goodfellow, Coraopolis, PA, USA). hERG currents were evoked using an activating pulse to +40 mV for 1000 ms followed by a tail current pulse to -50 mV for 2000 ms, and holding potential was -80 mV. Pulses were applied every 15 s, and all experiments were performed at room temperature. For the concentration response, peak tail current amplitude was measured during the voltage step to -50 mV.

**PK Mouse.** This study was performed with 42 naïve male CD1 mice, weighing 18–20 g upon arrival (4–5 weeks old). The first group of mice were dosed iv via a bolus in the tail vein with a dose level of 1 mg/kg, and the second group of mice was dosed orally as a single esophageal gavage with a dose level of 5 mg/kg.

Formulations were prepared the day before administration and kept at room temperature, protected from light. For the iv route, compound was formulated in PEG 200 and saline (60/40; v/v) as a clear solution. For the oral route, compound was formulated in PEG 200/purified water (60/40; v/v) as a homogeneous suspension. Before the oral dosing, the animals were deprived of food for at least 12 h before compound administration and 4 h after administration. All animals had free access to tap water.

From all animals, approximately 500  $\mu$ L blood samples were collected by intracardiac puncture and placed into tubes containing Li-heparin as anticoagulant. Blood samples were collected at the following time points: iv, 0.05, 0.25, 0.5, 1, 3, 5, and 8 h after dosing ( $n = 3$  mice per sampling time); po, 0.25, 0.5, 1, 3, 5, 8, and 24 h after dosing ( $n = 3$  mice per sampling time). Each mouse was sampled once and then euthanized.

Blood was kept on ice. Within 1 h after sampling, blood was centrifuged at 5000 rpm for 10 min at 4 °C. Immediately after centrifugation, the resulting plasma samples were collected into polypropylene tubes and were kept frozen at -20 °C pending bioanalysis.

Plasma samples were assayed by LC-MS/MS with a non-good-laboratory-practice (non-GLP)-validated method. Compound 36 plasma concentrations were calculated against a calibration curve consisting of eight levels with a 3 log amplitude. Back-calculated values for quality control (three levels prepared in duplicate) were used for accepting or rejecting the entire batch. The lower limit of quantification was 4 ng/mL with a plasma volume of 25  $\mu$ L.

Plasma proteins were precipitated with an excess of methanol containing the internal standard, and the corresponding supernatant was injected onto a C18 column. Analytes were eluted out of the HPLC system by increasing the percentage of the organic mobile phase. An API5500 QTrap mass spectrometer (AB Sciex, Sciex, Warrington, U.K.) was used for the simultaneous detection and quantification of 36.

PK parameters were calculated from the mean of individual plasma concentrations by noncompartmental analysis using WinNonlin software (Pharsight, version 5.2; Certara, Princeton, NJ, USA).

**PK Rat.** This study was performed with six naïve male Sprague Dawley rats, weighing 180–200 g upon arrival (6–8 weeks old). Catheterized rats (in the jugular vein) were used to avoid interindividual variability. Three rats per group was a sufficient number to carry out statistical calculations.

For the iv route, compound was formulated in PEG 200 and NaCl for injection (60/40; v/v) as a clear solution. For the oral route, compound was formulated in PEG 200 and purified water (60/40; v/v) as a clear solution.

Rats ( $n = 3$ ) were dosed iv via a bolus in the tail vein. Three additional rats were dosed orally as a single gavage. The iv bolus and the oral administration were given with a dose volume of 5 mL/kg. Actual dose volumes were based on the individual body weights.

From all animals, approximately 200  $\mu$ L blood samples were collected via a catheter into the jugular vein and placed into tubes containing Li-heparin as anticoagulant. Blood samples were collected at the following time points: iv, 0.05, 0.25, 0.5, 1, 3, 5, 8, and 24 h after dosing; po, 0.25, 0.5, 1, 3, 5, 8, and 24 h after dosing. Each rat was sampled seven or eight times (at each sampling time), depending on the route of administration. Just after each sampling, the same volume of physiological serum with sodium heparin (50 UI/mL) was injected into the catheter to avoid blocking.

Blood was kept on ice. Within 1 h after sampling, blood was centrifuged at 5000 rpm for 10 min at 4 °C. Immediately after centrifugation, the resulting plasma samples were collected into polypropylene tubes and were kept frozen at -20 °C pending bioanalysis.

Plasma samples were assayed by LC-MS/MS with a non-GLP-validated method. Plasma concentrations were calculated against a calibration curve consisting of eight levels with a 3 log amplitude. Back-calculated values for quality control (three levels prepared in duplicate) were used for accepting or rejecting the whole batch.

Plasma proteins were precipitated with an excess of methanol containing the internal standard, and the corresponding supernatant was injected on a C18 column. Analytes were eluted out the HPLC system by increasing the percentage of the organic mobile phase. An API5500 QTrap mass spectrometer (ABSciex, Sciex, Warrington, U.K.) was used.

PK parameters were calculated for each individual rat by noncompartmental analysis using WinNonlin software (Pharsight, version 5.2; Certara, Princeton, NJ, USA).

**PK Dog.** This study was performed with three non-naïve male Beagle dogs. Formulations were prepared the day of administration.

Dogs ( $n = 3$ ) were dosed iv via a 10 min infusion via a catheter with a dose level of 0.5 mg/kg (12 mL kg<sup>-1</sup> h<sup>-1</sup>). After a washout of 3 days, they were dosed orally as a single gavage with a dose level of 2.5 mg/kg in PEG200/water. The oral dose of 2.5 mg/kg was given with a dose volume of 5 mL/kg. Actual dose volumes were based on the individual body weights. Approximately 250 g of Harlan Teklad 2027 diet was distributed daily to each animal. The food was given 4 h after the iv administration. Before administration by the po route, animals were fasted for a period of at least 12 h before treatment, and food was given just after the 4 h blood sampling. All animals had free access to tap water.

From all animals approximately 0.5 mL blood samples were taken without anesthetic from a jugular or cephalic vein into tubes containing lithium heparin as anticoagulant. Blood samples were collected at the following time points: iv, at predose, 0.083, 0.167 (end of infusion), 0.5, 1, 2, 4, 6, 8, 10, and 24 h after start of infusion; po, at predose and then 0.25, 0.5, 1, 2, 3, 4, 6, 8, 10, and 24 h after dose administration.

Plasma samples were assayed by LC-MS/MS with a non-GLP-validated method. Compound 36 plasma concentrations were calculated against a calibration curve consisting of eight levels with a 3 log amplitude. Back-calculated values of the quality control samples (three levels prepared in duplicate) were used for accepting or rejecting the whole batch. The lower limit of quantification was 4 ng/mL with a plasma volume of 25  $\mu$ L.

Plasma proteins were precipitated with an excess of methanol containing the internal standard, and the corresponding supernatant was injected on a C18 column. Analytes were eluted out the high-performance liquid chromatography (HPLC) system by increasing the percentage of the organic mobile phase. An API5500 QTrap mass spectrometer (ABSciex, Sciex, Warrington, U.K.) was used for the detection and quantification of 36.

PK parameters were calculated for each individual dog by noncompartmental analysis using WinNonlin software (Pharsight, version 5.2; Certara, Princeton, NJ, USA).

**Negative Allosteric Modulation of Known GPR84 Agonists by GLPG1205. Membrane Preparation.** Membranes were generated from Flp-In T-REx 293 cells treated with 100 ng/mL doxycycline to induce expression of FLAG-GPR84-Gai2.<sup>32</sup> Cells were washed with ice-cold phosphate buffered saline, removed from dishes by scraping, and centrifuged at 3000 rpm for 5 min at 4 °C. Pellets were resuspended in TE buffer (10 mM Tris-HCl, 0.1 mM EDTA; pH 7.5) containing a protease inhibitor mixture (Roche Applied Science, West Sussex, U.K.) and homogenized with a 5 mL hand-held homogenizer. This material was centrifuged at 1500 rpm for 5 min at 4 °C, and the supernatant was further centrifuged at 50 000 rpm for 30 min at 4 °C. The resulting pellet was resuspended in TE buffer, and protein content was assessed using a BCA protein assay kit (Pierce, Fisher Scientific, Loughborough, U.K.).

**Competition Binding Assay.** Assays were performed using 0.2 nM [<sup>3</sup>H]38, binding buffer (phosphate-buffered saline with 0.5% fatty acid free bovine serum albumin; pH 7.4) and the indicated concentrations of test compounds, in a total assay volume of 500  $\mu$ L. Binding was initiated by the addition of membranes (5  $\mu$ g of protein per tube), and incubations were carried out at 25 °C for 1 h. Reactions were terminated by the addition of ice-cold phosphate buffered saline and vacuum filtration through GF/C glass filters using a 24-well Brandel cell harvester (Alpha Biotec, Glasgow, U.K.). Each reaction tube was washed three times with ice-cold PBS. The filters were allowed to dry for 2–3 h and then placed in 3 mL of Ultima Gold XR. Radioactivity was quantified by liquid scintillation spectrometry.

**Reaction Biology Kinase Selectivity Profiling.** Inhibition of 152 kinases by 10  $\mu$ M compound was determined in a Reaction Biology proprietary nanoliter radioactive HotSpot assay in duplicate. The principle of the assay consists of the measurement of incorporated <sup>33</sup>P into a specific substrate for each kinase when the substrate is phosphorylated by the enzyme using [<sup>33</sup>P]- $\gamma$ -ATP and ATP.

**Millipore GPCR Profiler Selectivity Profiling.** Free intracellular [Ca<sup>2+</sup>] flux assays were conducted to test compound agonist and antagonist activities against 123 GPCRs selected to cover as many GPCR families as possible. Percentage activation was determined upon initial addition of compound followed by 10 min incubation at 25 °C (in absence of agonist). Following this initial incubation, reference agonists were added at EC<sub>80</sub> concentration allowing determination of percentage inhibition of the agonist induced signal caused by compound.

**Dextran Sulfate Sodium (DSS)-Induced Colitis Model.** Balb/cj female mice (Janvier Labs, Le Genest-Saint-Isle, France) were housed in a dedicated in house animal facility under specific pathogen-free conditions according to the Federation for Laboratory Animal Science Associations guidelines. The study was performed according to ethical guidelines approved by the Animal Institutional Care and Use Committee of Galapagos controlled by the French Authorities (Agreement No. C93-063-06, DDPP, Seine Saint Denis). Animals were housed in filter top cages, provided with filtered tap water and standard chow ad libitum, and maintained at 22  $\pm$  2 °C in 55  $\pm$  10% humidity on a 12 h light/dark cycle. The randomization of mice in the different groups was based on body weight (BW) at study commencement. A model of chronic colitis was induced in 8-week-old mice (BW 25 g) with three cycles, each consisting of 4% DSS administered in drinking water for 4 days, followed by 3 days of regular drinking water. The mice ( $n$  = 10 per group) were orally administered vehicle (PEG200/H<sub>2</sub>O [60/40; v/v]) or 1, 3, or 10 mg/kg of compounds 26, 35, 36 qd from day 1 of DSS administration and throughout the dosing period. Compound 36 was tested in three independent experiments. Two positive controls were used in these different studies: cyclosporine (CsA) at 25 mg/kg qd po in PEG200/water (60/40; v/v) or sulfasalazine at 20 mg/kg qd po in 0.5% methylcellulose. Clinical parameters were measured every other day. DAI (a combined score of body weight loss, stool consistency, and

rectal bleeding scores) was recorded daily. Each criterion was graded from 0 to 4. Animals were decapitated after brief isoflurane anesthesia. At necropsy at day 17 of the experiment, the complete colon was removed and rinsed with sterile PBS. A segment of 5 mm of distal colon was collected for histology analysis. Histology was performed on formalin-fixed (4% buffered formaldehyde for 3 h). After fixation, samples were transferred into a sucrose solution prior to being frozen in isopentane. Three series of cryosections within a distance of 1 mm were performed in duplicate. One series of sections were stained with a Goldner trichrome for colon lesion evaluation, and scoring was performed. Neutrophil cell infiltration was assayed by immunohistochemistry using anti-Ly6G/Ly6C (clone NIMP-R14, Santa Cruz, Dallas, TX, USA). Neutrophil identification was followed by manual quantification of cell number per surface. The neutrophil density was expressed as a number of cells per mm<sup>2</sup> of colon area. Blood was sampled at day 4 at four time points: 0, 1, 3, and 6 h (and assuming 24 h is equal to the predose sample). Plasma was prepared and 36 was quantified using LC–MS to assess steady state PK. Statistical analysis was performed with Prism 5.03 software (GraphPad, San Diego, CA, USA) with a one-way ANOVA performed on the arcsinh(log)-transformed neutrophil density data and a two-way ANOVA performed on the arcsinh(log)-transformed DAI data. Dunnett's post-hoc multiplicity correction procedure was applied to the neutrophil density data, and Bonferonni post-hoc multiplicity correction procedure was applied to the DAI data.

## ■ ASSOCIATED CONTENT

### Supporting Information

The Supporting Information is available free of charge at <https://pubs.acs.org/doi/10.1021/acs.jmedchem.0c00272>.

General methods and synthetic routes used in the investigation of compounds; synthetic procedures and analytical data for all compounds (PDF)

Molecular formula strings and some data (CSV)

## ■ AUTHOR INFORMATION

### Corresponding Author

Romain Gosmini – Galapagos SASU, 93230 Romainville, France; Phone: +33149424778; Email: [romain.gosmini@glpg.com](mailto:romain.gosmini@glpg.com)

### Authors

Frédéric Labégère – Galapagos SASU, 93230 Romainville, France

Sonia Dupont – Galapagos SASU, 93230 Romainville, France

Luke Alvey – Galapagos SASU, 93230 Romainville, France

Florilène Soulas – Galapagos SASU, 93230 Romainville, France

Gregory Newsome – Galapagos SASU, 93230 Romainville, France

Amynata Tirera – Galapagos SASU, 93230 Romainville, France

Vanessa Quenehen – Galapagos SASU, 93230 Romainville, France

Thi Thu Trang Mai – Galapagos SASU, 93230 Romainville, France

Pierre Deprez – Galapagos SASU, 93230 Romainville, France

Roland Blanqué – Galapagos SASU, 93230 Romainville, France

Line Oste – Galapagos NV, 2800 Mechelen, Belgium

Sandrine Le Tallec – Galapagos SASU, 93230 Romainville, France

Steve De Vos – Galapagos NV, 2800 Mechelen, Belgium

Annick Hagers – Galapagos NV, 2800 Mechelen, Belgium

Ann Vandeveldt – Galapagos NV, 2800 Mechelen, Belgium

Luc Nelles – Galapagos NV, 2800 Mechelen, Belgium  
Nele Vandervoort – Galapagos NV, 2800 Mechelen, Belgium  
Katja Conrath – Galapagos NV, 2800 Mechelen, Belgium  
Thierry Christophe – Galapagos NV, 2800 Mechelen, Belgium  
Ellen van der Aar – Galapagos NV, 2800 Mechelen, Belgium  
Emanuelle Wakselman – Galapagos SASU, 93230 Romainville, France  
Didier Merciris – Galapagos SASU, 93230 Romainville, France  
Céline Cottreaux – Galapagos SASU, 93230 Romainville, France  
Cécile da Costa – Galapagos SASU, 93230 Romainville, France  
Laurent Saniere – Galapagos SASU, 93230 Romainville, France  
Philippe Clement-Lacroix – Galapagos SASU, 93230 Romainville, France  
Laura Jenkins – Centre for Translational Pharmacology, Institute of Molecular, Cell and Systems Biology, College of Medical Veterinary and Life Sciences, University of Glasgow, Glasgow G12 8QQ, United Kingdom  
Graeme Milligan – Centre for Translational Pharmacology, Institute of Molecular, Cell and Systems Biology, College of Medical Veterinary and Life Sciences, University of Glasgow, Glasgow G12 8QQ, United Kingdom; [orcid.org/0000-0002-6946-3519](https://orcid.org/0000-0002-6946-3519)  
Stephen Fletcher – Galapagos NV, 2800 Mechelen, Belgium  
Reginald Brys – Galapagos NV, 2800 Mechelen, Belgium

Complete contact information is available at:  
<https://pubs.acs.org/10.1021/acs.jmedchem.0c00272>

### Author Contributions

All authors' provided substantial contributions to the design or the acquisition, analysis, or interpretation of data. Authors critically reviewed the manuscript for important intellectual content. All authors read and approved the final version of the manuscript.

### Funding

This study and the medical writing support were funded by Galapagos.

### Notes

The authors declare the following competing financial interest(s): S. Dupont, L. Alvey, G. Newsome, A. Tirera, V. Quenehen, T. T. T. Mai, P. Deprez, R. Blanque, E. Wakselman, S. Le Tallec, D. Merciris, C. Cottreaux, C. da Costa, L. Saniere, P. Clement-Lacroix, and R. Gosmini are employees of Galapagos SASU, France. S. De Vos, A. Hagers, A. Vandeveld, L. Nelles, N. Vandervoort, K. Conrath, T. Christophe, E. van der Aar, L. Oste, and R. Brys are employees of Galapagos NV, Belgium. F. Labeguere, F. Soulas, and S. Fletcher are former employees of Galapagos. G. Milligan has received funding and support from Galapagos NV, Belgium. L. Jenkins has no conflicts of interest.

### ACKNOWLEDGMENTS

Medical writing assistance in the preparation of this manuscript was provided by Emily Fisher, Alexander Bowen and Samuel McCracken of CircleScience (an Ashfield Company, part of UDG Healthcare plc) and funded by Galapagos. The authors thank Sebastien Richard for his support in the development of the analytical chemistry section.

### ABBREVIATIONS USED

ADME, absorption, distribution, metabolism, excretion; ASOL, aqueous solubility;  $AUC_{0-\infty}$ , area under the curve (from time 0 to infinity); BEH, ethylene bridged hybrid; BSA, bovine serum albumin; BW, body weight; cAMP, cyclic adenosine 3',5'-monophosphate; Cap, capric acid; CAS, Chemical Abstracts Service; CL, clearance;  $CL_{int}$ , intrinsic clearance;  $CL_{unb}$ , unbound clearance;  $C_{max}$ , maximum plasma concentration; compd, compound; cpm, counts per minute;  $C_0$ , concentration extrapolated at time 0 after a bolus intravenous dose; D, dog; DAI, disease activity index; DIM, 3,3'-diindolylmethane; DMSO, dimethyl sulfoxide; DSS, dextran sodium sulfate; ECACC, European Collection of Cell Cultures;  $EC_{50}$ , half maximal effective concentration;  $EC_{80}$ , concentration of agonist leading to 80% maximal response; EGTA, ethylene glycol-bis( $\beta$ -aminoethyl ether)- $N,N,N',N'$ -tetraacetic acid; ER, efflux ratio; F, oral bioavailability; GPCR, G-protein-coupled receptor; GTP $\gamma$ S, guanosine 5'-O-[ $\gamma$ -thio]triphosphate; h, hour; HBSS, Hanks' balanced salt solution; hCYP, human cytochrome P450; HEP, hepatocyte; HEPES, (4-(2-hydroxyethyl)-1-piperazineethanesulfonic acid; hERG, human ether-à-go-go-related gene; hGPR84, human G-protein-coupled receptor 84; hGTP $\gamma$ S, human guanosine 5'-O-[ $\gamma$ -thio]triphosphate; HLM, human liver microsome; HTRF, homogeneous time-resolved fluorescence; HTS, high-throughput screen; Hum neutro, human neutrophil migration assay; H, human; IBD, inflammatory bowel disease; IBMX, 3-isobutyl-1-methylxanthine;  $IC_{50}$ , half maximal inhibitory concentration; IL, interleukin; IP1, inositol monophosphate; iv, intravenous; LCMS/MS, liquid chromatography–mass spectrometry/mass spectrometry; LMS, liver microsomal stability; M, mouse; MCFA, medium-chain free fatty acid; Me, methyl group; MED, minimal efficacious dose; MELK, maternal embryonic leucine zipper kinase; MIC, microsomal; min, minute; mRNA, messenger ribonucleic acid; MW, molecular weight; NMR, nuclear magnetic resonance; OBD, optical bed density;  $P_{app}$ ,  $A_2B$ , apparent permeability from apical to basal chambers; PDA, photodiode array; PDE4A, phosphodiesterase 4; PEG, polyethylene glycol; PK, pharmacokinetics; PPB, plasma protein binding; po, per os;  $POCl_3$ , phosphoryl chloride; PSA, polar surface area; qd, once daily; R, rat; rpm, revolutions per minute; RT, room temperature; SAR, structure–activity relationship; SPA, scintillation proximity assay; SQD, single quadrupole detection;  $T_{1/2}$ , half-life;  $T_{max}$ , time at maximum plasma concentration; TNF- $\alpha$ , tumor necrosis factor  $\alpha$ ; UPLC, ultraperformance liquid chromatography; UV, ultraviolet;  $V_{ss}$ , apparent volume of distribution at steady state

### REFERENCES

- (1) Wang, J.; Wu, X.; Simonavicius, N.; Tian, H.; Ling, L. Medium-chain fatty acids as ligands for orphan G protein-coupled receptor GPR84. *J. Biol. Chem.* **2006**, *281* (45), 34457–34464.
- (2) Davenport, A. P.; Alexander, S. P.; Sharman, J. L.; Pawson, A. J.; Benson, H. E.; Monaghan, A. E.; Liew, W. C.; Mpamhanga, C. P.; Bonner, T. I.; Neubig, R. R.; Pin, J. P.; Spedding, M.; Harmar, A. J. International Union of Basic and Clinical Pharmacology. LXXXVIII. G protein-coupled receptor list: recommendations for new pairings with cognate ligands. *Pharmacol. Rev.* **2013**, *65* (3), 967–986.
- (3) Suzuki, M.; Takaishi, S.; Nagasaki, M.; Onozawa, Y.; Iino, I.; Maeda, H.; Komai, T.; Oda, T. Medium-chain fatty acid-sensing receptor, GPR84, is a proinflammatory receptor. *J. Biol. Chem.* **2013**, *288* (15), 10684–10691.
- (4) Liu, Y.; Zhang, Q.; Chen, L. H.; Yang, H.; Lu, W.; Xie, X.; Nan, F. J. Design and synthesis of 2-alkylpyrimidine-4,6-diol and 6-

alkylpyridine-2,4-diol as potent GPR84 agonists. *ACS Med. Chem. Lett.* **2016**, *7* (6), 579–583.

(5) Zhang, Q.; Yang, H.; Li, J.; Xie, X. Discovery and characterization of a novel small-molecule agonist for medium-chain free fatty acid receptor G protein-coupled receptor 84. *J. Pharmacol. Exp. Ther.* **2016**, *357* (2), 337–344.

(6) Pillaiyar, T.; Kose, M.; Namasivayam, V.; Sylvester, K.; Borges, G.; Thimm, D.; von Kugelgen, I.; Muller, C. E. 6-(Ar)alkylamino-substituted uracil derivatives: lipid mimetics with potent activity at the orphan G protein-coupled receptor 84 (GPR84). *ACS omega* **2018**, *3* (3), 3365–3383.

(7) Yousefi, S.; Cooper, P. R.; Potter, S. L.; Mueck, B.; Jarai, G. Cloning and expression analysis of a novel G-protein-coupled receptor selectively expressed on granulocytes. *Journal Leukocyte Biol.* **2001**, *69* (6), 1045–1052.

(8) Lattin, J. E.; Schroder, K.; Su, A. I.; Walker, J. R.; Zhang, J.; Wiltshire, T.; Saijo, K.; Glass, C. K.; Hume, D. A.; Kellie, S.; Sweet, M. J. Expression analysis of G protein-coupled receptors in mouse macrophages. *Immunome Res.* **2008**, *4*, 5.

(9) Audoy-Remus, J.; Bozoyan, L.; Dumas, A.; Filali, M.; Lecours, C.; Lacroix, S.; Rivest, S.; Tremblay, M. E.; Vallieres, L. GPR84 deficiency reduces microgliosis, but accelerates dendritic degeneration and cognitive decline in a mouse model of Alzheimer's disease. *Brain, Behav., Immun.* **2015**, *46*, 112–120.

(10) Bouchard, C.; Page, J.; Bedard, A.; Tremblay, P.; Vallieres, L. G protein-coupled receptor 84, a microglia-associated protein expressed in neuroinflammatory conditions. *Glia* **2007**, *55* (8), 790–800.

(11) Venkataraman, C.; Kuo, F. The G-protein coupled receptor, GPR84 regulates IL-4 production by T lymphocytes in response to CD3 crosslinking. *Immunol. Lett.* **2005**, *101* (2), 144–153.

(12) Nagasaki, H.; Kondo, T.; Fuchigami, M.; Hashimoto, H.; Sugimura, Y.; Ozaki, N.; Arima, H.; Ota, A.; Oiso, Y.; Hamada, Y. Inflammatory changes in adipose tissue enhance expression of GPR84, a medium-chain fatty acid receptor: TNF $\alpha$  enhances GPR84 expression in adipocytes. *FEBS Lett.* **2012**, *586* (4), 368–372.

(13) Nicol, L. S.; Dawes, J. M.; La Russa, F.; Didangelos, A.; Clark, A. K.; Gentry, C.; Grist, J.; Davies, J. B.; Malcangio, M.; McMahon, S. B. The role of G-protein receptor 84 in experimental neuropathic pain. *J. Neurosci.* **2015**, *35* (23), 8959–8969.

(14) Sundqvist, M.; Christenson, K.; Holdfeldt, A.; Gabl, M.; Mårtensson, J.; Björkman, L.; Dieckmann, R.; Dahlgren, C.; Forsman, H. Similarities and differences between the responses induced in human phagocytes through activation of the medium chain fatty acid receptor GPR84 and the short chain fatty acid receptor FFA2R. *Biochim. Biophys. Acta, Mol. Cell Res.* **2018**, *1865* (5), 695–708.

(15) Arijis, I.; De Hertogh, G.; Machiels, K.; Van Steen, K.; Lemaire, K.; Schraenen, A.; Van Lommel, L.; Quintens, R.; Van Assche, G.; Vermeire, S.; Schuit, F.; Rutgeerts, P. Mucosal gene expression of cell adhesion molecules, chemokines, and chemokine receptors in patients with inflammatory bowel disease before and after infliximab treatment. *Am. J. Gastroenterol.* **2011**, *106* (4), 748–761.

(16) Gagnon, L.; Leduc, M.; Thibodeau, J. F.; Zhang, M. Z.; Grouix, B.; Sarra-Bournet, F.; Gagnon, W.; Hince, K.; Tremblay, M.; Geerts, L.; Kennedy, C. R. J.; Hebert, R. L.; Gutsol, A.; Holterman, C. E.; Kamto, E.; Gervais, L.; Ouboudinar, J.; Richard, J.; Felton, A.; Laverdure, A.; Simard, J. C.; Letourneau, S.; Cloutier, M. P.; Leblond, F. A.; Abbott, S. D.; Penney, C.; Duceppe, J. S.; Zacharie, B.; Dupuis, J.; Calderone, A.; Nguyen, Q. T.; Harris, R. C.; Laurin, P. A newly discovered antifibrotic pathway regulated by two fatty acid receptors: GPR40 and GPR84. *Am. J. Pathol.* **2018**, *188* (5), 1132–1148.

(17) Abdel-Aziz, H.; Schneider, M.; Neuhuber, W.; Meguid Kassem, A.; Khailah, S.; Muller, J.; Gamal Eldeen, H.; Khairy, A.; Khayyal, M. T.; Shcherbakova, A.; Efferth, T.; Ulrich-Merzenich, G. GPR84 and TREM-1 signaling contribute to the pathogenesis of reflux esophagitis. *Mol. Med.* **2015**, *21* (1), 1011–1024.

(18) Dietrich, P. A.; Yang, C.; Leung, H. H.; Lynch, J. R.; Gonzales, E.; Liu, B.; Haber, M.; Norris, M. D.; Wang, J.; Wang, J. Y. GPR84 sustains aberrant beta-catenin signaling in leukemic stem cells for

maintenance of MLL leukemogenesis. *Blood* **2014**, *124* (22), 3284–3294.

(19) Du Toit, E.; Browne, L.; Irving-Rodgers, H.; Massa, H. M.; Fozzard, N.; Jennings, M. P.; Peak, I. R. Effect of GPR84 deletion on obesity and diabetes development in mice fed long chain or medium chain fatty acid rich diets. *Eur. J. Nutr.* **2018**, *57* (5), 1737–1746.

(20) Mignani, S.; Rodrigues, J.; Tomas, H.; Jalal, R.; Singh, P. P.; Majoral, J. P.; Vishwakarma, R. A. Present drug-likeness filters in medicinal chemistry during the hit and lead optimization process: how far can they be simplified? *Drug Discovery Today* **2018**, *23* (3), 605–615.

(21) Kodimuthali, A.; Jabaris, S. S. L.; Pal, M. Recent advances on phosphodiesterase 4 inhibitors for the treatment of asthma and chronic obstructive pulmonary disease. *J. Med. Chem.* **2008**, *51* (18), 5471–5489.

(22) Niu, M.; Dong, F.; Tang, S.; Fida, G.; Qin, J.; Qiu, J.; Liu, K.; Gao, W.; Gu, Y. Pharmacophore modeling and virtual screening for the discovery of new type 4 cAMP phosphodiesterase (PDE4) inhibitors. *PLoS One* **2013**, *8* (12), e82360.

(23) Oxford, A. W.; Jack, D. Derivatives of Pyrimido[6,1-A]isoquinolin-4-One. WO/2000/058309, Mar 29, 2000; <https://patentscope.wipo.int/search/en/detail.jsf?docId=WO2000058309>.

(24) Sina, C.; Gavrilo, O.; Förster, M.; Till, A.; Derer, S.; Hildebrand, F.; Raabe, B.; Chalaris, A.; Scheller, J.; Rehmann, A.; Franke, A.; Ott, S.; Häslar, R.; Nikolaus, S.; Fölsch, U. R.; Rose-John, S.; Jiang, H. P.; Li, J.; Schreiber, S.; Rosenstiel, P. G protein-coupled receptor 43 is essential for neutrophil recruitment during intestinal inflammation. *J. Immunol.* **2009**, *183* (11), 7514–7522.

(25) Wirtz, S.; Neufert, C.; Weigmann, B.; Neurath, M. F. Chemically induced mouse models of intestinal inflammation. *Nat. Protoc.* **2007**, *2* (3), 541–546.

(26) Mahmud, Z. A.; Jenkins, L.; Ulven, T.; Labéguère, F.; Gosmini, R.; De Vos, S.; Hudson, B. D.; Tikhonova, I. G.; Milligan, G. Three classes of ligands each bind to distinct sites on the orphan G protein-coupled receptor GPR84. *Sci. Rep.* **2017**, *7* (1), 17953.

(27) Kim, H. Y.; Kuhn, R. J.; Patkar, C.; Warriar, R.; Cushman, M. Synthesis of dioxane-based antiviral agents and evaluation of their biological activities as inhibitors of Sindbis virus replication. *Bioorg. Med. Chem.* **2007**, *15* (7), 2667–2679.

(28) Vanhoutte, F.; Dupont, S.; Van Kaem, T.; Gouy, M.-H.; Gheyle, L.; Blanque, R.; Brys, R.; Vandeghinste, N.; Haazen, W.; van't Klooster, G.; Beetens, J. Human safety, pharmacokinetics and pharmacodynamics of the GPR84 antagonist GLPG1205, a potential new approach to treat IBD. *United Eur. Gastroenterol. J.* **2014**, *2* (1S), A224 (Abstract P0341).

(29) Galapagos Reports Results with GLPG1205 in Ulcerative Colitis. Galapagos Press Release January 26, 2016. [https://cws.huginonline.com/G/133350/PR/201601/1981193\\_5.html](https://cws.huginonline.com/G/133350/PR/201601/1981193_5.html) (accessed Apr 3, 2019).

(30) Puengel, T.; De Vos, S.; Hundertmark, J.; Kohlhepp, M.; Guldiken, N.; Pujuguet, P.; Auberval, M.; Marsais, F.; Shoji, K. F.; Saniere, L.; Trautwein, C.; Luedde, T.; Strnad, P.; Brys, R.; Clement-Lacroix, P.; Tacke, F. The medium-chain fatty acid receptor GPR84 mediates myeloid cell infiltration promoting steatohepatitis and fibrosis. *J. Clin. Med.* **2020**, *9* (4), E1140.

(31) Saniere, L.; Marsais, F.; Jagerschmidt, C.; Meurisse, S.; Cuzic, S.; Shoji, K.; Clement-Lacroix, P.; Van Osselaer, N.; De Vos, S. Characterization of GLPG1205 in mouse fibrosis models: a potent and selective antagonist of GPR84 for treatment of idiopathic pulmonary fibrosis. *Am. J. Respir. Crit. Care Med.* **2019**, *199*, A1046.

(32) Mancini, S.J.; Al Mahmud, Z.; Jenkins, L.; Bolognini, D.; Newman, R.; Barnes, M.; Edye, M. E.; McMahon, S. B.; Tobin, A.; Milligan, G. On-target and off-target effects of novel orthosteric and allosteric activators of GPR84. *Sci. Rep.* **2019**, *9* (1), 1861.